Cell Reports

Article

The f subunit of human ATP synthase is essential for normal mitochondrial morphology and permeability transition

Graphical abstract

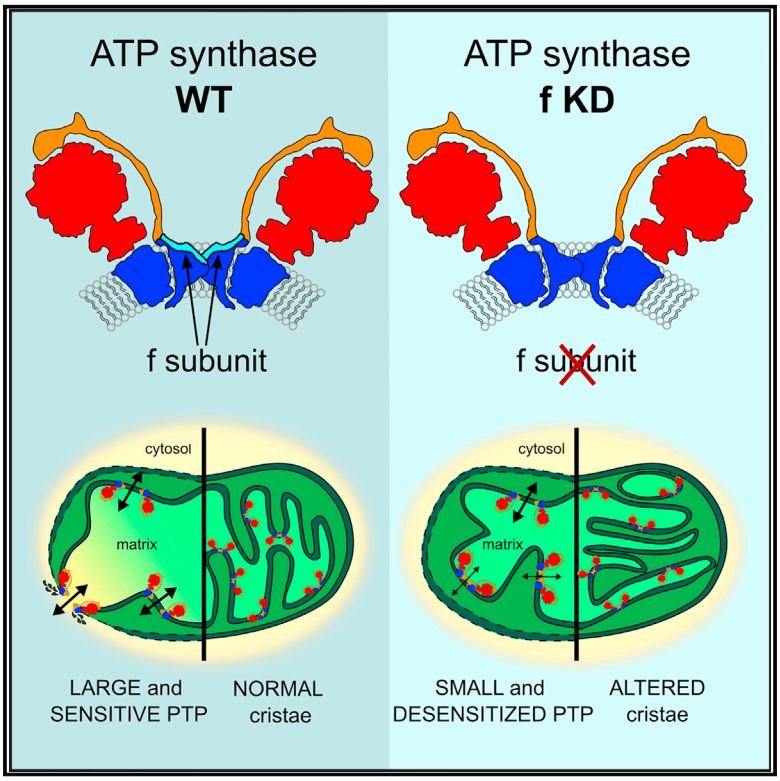

Authors

Chiara Galber, Giovanni Minervini, Giuseppe Cannino, ..., Silvio Tosatto, Giovanna Lippe, Valentina Giorgio

Correspondence

valentina.giorgio4@unibo.it

In brief

Galber et al. determine the roles of the ATP synthase f subunit in mitochondria. They demonstrate that f subunit downregulation disrupts normal crista morphology and modulates the size and sensitivity of the permeability transition pore without affecting enzymatic activity or the stoichiometry of other subunits.

Highlights

- The f subunit is essential for ATP synthase dimer (but not monomer) stability
- ATP synthase synthetic/hydrolytic activity is unaltered in f subunit knockdown cells
- Downregulation of the human f subunit disrupts normal crista morphology
- The f subunit modulates size and sensitivity of the permeability transition pore

Galber et al., 2021, Cell Reports *35*, 109111
May 11, 2021
https://doi.org/10.1016/j.celrep.2021.109111

CellPress

Cell Reports

CellPress
OPEN ACCESS

Article

The f subunit of human ATP synthase is essential for normal mitochondrial morphology and permeability transition

Chiara Galber,[1,2] Giovanni Minervini,[1] Giuseppe Cannino,[1] Francesco Boldrin,[3] Valeria Petronilli,[1,2] Silvio Tosatto,[1] Giovanna Lippe,[4] and Valentina Giorgio[1,2,5,6,*]

[1]Department of Biomedical Sciences, University of Padova, Padova 35121, Italy
[2]Consiglio Nazionale delle Ricerche Institute of Neuroscience, Padova 35121, Italy
[3]Department of Biology, University of Padova, Padova 35121, Italy
[4]Department of Medicine, University of Udine, Udine 33100, Italy
[5]Department of Biomedical and Neuromotor Sciences, University of Bologna, Bologna 40126, Italy
[6]Lead contact
*Correspondence: valentina.giorgio4@unibo.it
https://doi.org/10.1016/j.celrep.2021.109111

SUMMARY

The f subunit is localized at the base of the ATP synthase peripheral stalk. Its function in the human enzyme is poorly characterized. Because full disruption of its *ATP5J2* gene with the CRISPR-Cas9 strategy in the HAP1 human model has been shown to cause alterations in the amounts of other ATP synthase subunits, here we investigated the role of the f subunit in HeLa cells by regulating its levels through RNA interference. We confirm the role of the f subunit in ATP synthase dimer stability and observe that its downregulation per se does not alter the amounts of the other enzyme subunits or ATP synthase synthetic/hydrolytic activity. We show that downregulation of the f subunit causes abnormal crista organization and decreases permeability transition pore (PTP) size, whereas its re-expression in f subunit knockdown cells rescues mitochondrial morphology and PTP-dependent swelling.

INTRODUCTION

ATP synthase is known as a nanomotor that synthesizes ATP (Boyer, 2000) by using the electrochemical gradient generated across the inner mitochondrial membrane during respiration, according to the chemiosmotic theory (Mitchell, 1961). When the proton gradient collapses, the enzyme can work in reverse by hydrolyzing ATP and restoring the membrane potential (Myers and Slater, 1957a, 1957b). ATP synthase determines the so-called "rotary catalysis" (Stock et al., 1999). The enzyme can be divided into a membrane sector (Fo), where it is known that the a and c subunits contribute to proton translocation through the membrane, and a soluble part (F_1), which contains the sites where ATP, ADP, and Pi bind (Abrahams et al., 1994; Harris, 1993). The F_1 and Fo sectors are connected in the native complex by central and peripheral stalks. The bovine peripheral stalk is formed by subunits oligomycin-sensitivity-conferring protein (OSCP), b, F6, and d (Rees et al., 2009). The N-terminal domain of subunit f (Guo et al., 2017), subunits i/j (Srivastava et al., 2018) of the yeast species, and the C-terminal region of subunit A6L of the yeast and bovine complex (Lee et al., 2015; Guo et al., 2017) have been assigned to the base of the peripheral stalk. The interactions between the peripheral stalk and the Fo subunits ensure structural and functional coupling between F_O and F_1 sectors. Studies in yeast have proposed that the f and i/j subunits participate in formation of ATP synthase dimers (Hahn et al., 2016; Guo et al., 2017), indicating that they might contribute to stabilize the monomer-monomer interface together with the a, b, e, and g subunits (Habersetzer et al., 2013; Wittig et al., 2008). In the porcine, ovine, and bovine enzymes, the contacts of the f subunit with the aforementioned a, b, e, and g subunits have been characterized recently by cryoelectron microscopy (cryo-EM) studies (Gu et al., 2019; Pinke et al., 2020; Spikes et al., 2020), suggesting that the f subunit also stabilizes dimers in mammals.

Dimers and oligomers of ATP synthase have been described in mitochondria of different species (Daum et al., 2013; Davies et al., 2011; Dudkina et al., 2010, 2006; Strauss et al., 2008; von Stockum et al., 2015; Wittig et al., 2010). Dimers are predicted to generate a high local curvature in the inner mitochondrial membrane (Blum et al., 2019; Strauss et al., 2008), affecting crista morphology. Decreased dimer stability has been found in yeast mitochondria lacking the e and g subunits or expressing a modified b subunit (truncated in its N-terminal part or deleted in its intermembrane space loop) and displaying an "onion-like" structure (Arselin et al., 2004; Giraud et al., 2002; Velours et al., 2009; Weimann et al., 2008). In human cells, subunits e and g are also essential for dimer stability, and their lack causes major defects in mitochondrial morphology (Habersetzer et al., 2013). Involvement in crista morphology of the other Fo subunits, a and f or the yeast-specific i/j, has not yet been determined.

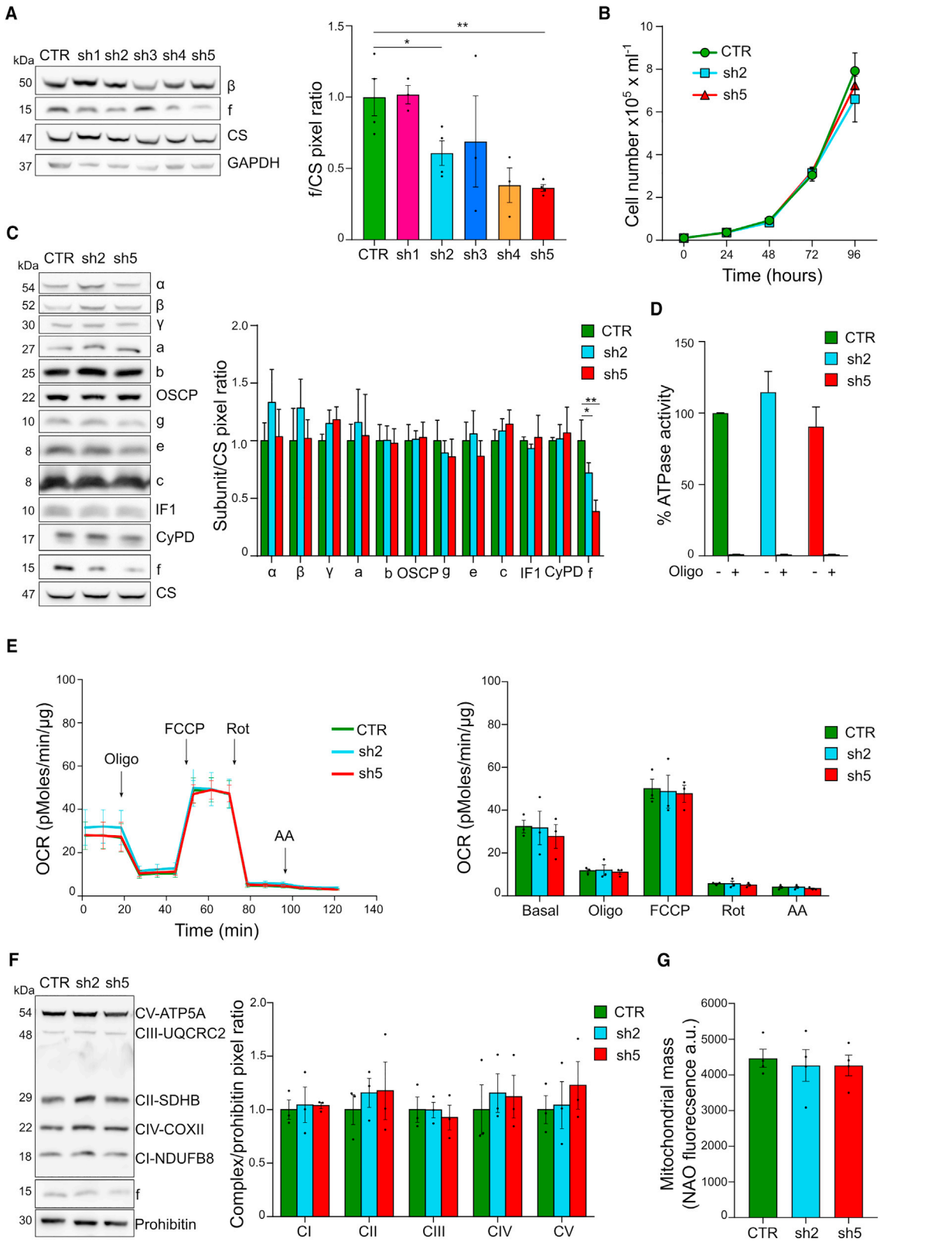

(legend on next page)

ATP synthase dimers/oligomers have been hypothesized to form the permeability transition (PT) pore (PTP) (Giorgio et al., 2013). This is a Ca^{2+}-dependent megachannel with an estimated diameter of 30 Å, large enough to allow diffusion of solutes up to about 1,500 Da (Bernardi et al., 2015), that was characterized by electrophysiology (Petronilli et al., 1989; Szabó et al., 1992; Szabó and Zoratti, 1991). This approach showed that ATP synthases extracted from mammals, *Saccharomyces cerevisiae*, and *Drosophila melanogaster* form channels with the properties expected for the corresponding PTPs (Alavian et al., 2014; Carraro et al., 2014; Giorgio et al., 2013; Neginskaya et al., 2019; von Stockum et al., 2015).

So far, although the involvement of ATP synthase in PT is still being debated (He et al., 2017a, 2017b), results obtained by genetic manipulation of enzyme components have revealed modulatory mechanisms of the channel (Antoniel et al., 2018; Carraro et al., 2018; Giorgio et al., 2017; Guo et al., 2019, 2018; Lee et al., 2016; Neginskaya et al., 2019). Importantly, the e, g, and b subunits modulate the size of the Ca^{2+}-activated channel in yeast (Carraro et al., 2018), suggesting that the Fo region participates in PT. An additional candidate for formation of the channel is the f subunit because of (1) its key localization at the base of the peripheral stalk in close proximity to the putative channel-forming subunits b, e, and g (Gu et al., 2019; Spikes et al., 2020) and (2) its conserved C-terminal hydrophilic end, which was not resolved in the cryo-EM studies by Srivastava et al. (2018) and Guo et al. (2017), suggesting its high motility.

The f subunit appears as an integral inner membrane protein of about 10 kDa (Collinson et al., 1994; Velours et al., 1998). The f subunit contacts subunits e, g, A6L, and 6.8PL (Belogrudov et al., 1996; Lee et al., 2015) and a and b (Velours et al., 1998), as revealed by cross-linking in the bovine or yeast enzyme, respectively. These finding were confirmed by cryo-EM in *Yarrowia lipolytica*, *S. cerevisiae*, *Sus scrofa*, *Bos taurus*, and *Ovis aries* (Gu et al., 2019; Guo et al., 2017; Hahn et al., 2016; Pinke et al., 2020; Spikes et al., 2020; Srivastava et al., 2018). In yeast, lack of the f subunit is lethal (Spannagel et al., 1997). In haploid HAP1 human cells, disruption of the *ATP5J2* gene encoding the f subunit causes alterations in ATP synthase assembly and in dimer stability (He et al., 2018). In these *ATP5J2* knockout clones, lack of the f subunit causes changes in the protein level of other ATP synthase subunits and respiratory chain complexes, a phenotype that makes it difficult to predict a role of the f subunit. For this reason, in the present study, we investigated the role of the human f subunit in modulation of ATP synthesis/hydrolysis, mitochondrial morphology, and PT in HeLa cells by regulating f subunit levels through RNA interference.

RESULTS

Knocking down the f subunit does not affect ATP synthesis/hydrolysis or ATP synthase subunit stoichiometry in high-glucose medium

Ablation of the f subunit in f-null human clones causes alterations in ATP synthase subunit stoichiometry and in the amount of respiratory chain components (He et al., 2018). We generated a different human model in which the f subunit level is downregulated through lentiviral infection with different shRNA sequences. The obtained HeLa cell mixed populations showed a different decrease of the f subunit, as revealed by western blotting (Figure 1A), with the exception of sh1 cells, as shown by normalization on the right. Citrate synthase (CS) and glyceraldehyde 3-phosphate dehydrogenase (GAPDH) were used as mitochondrial and cytosolic loading controls, respectively. HeLa sh2 and sh5 cells showed a progressive decrease in f subunit levels, which were quantified as 30% and 70% of the control, respectively (Figure 1A). These cells did not show any difference in their growth rate compared with controls (Figure 1B). The amounts of the subunits α, β, γ, a, b, OSCP, g, e, and c and the content of the endogenous inhibitor protein IF1 (Green and Grover, 2000), which plays a prominent role in enzyme activity regulation (Di Pancrazio et al., 2004), were unchanged in HeLa sh2 and sh5 cells and their controls (Figure 1C). The levels of cyclophilin D

Figure 1. f subunit KD does not alter ATP synthase subunit composition, ATP synthesis/hydrolysis, or OXPHOS components in HeLa cells grown in a high-glucose-containing medium

(A) Western blot (left panel) of citrate synthase (CS), glyceraldehyde 3-phosphate dehydrogenase (GAPDH), the ATP synthase subunits f and β, and mean ratio between f and CS band pixels (right panel) in control (CTR) or f subunit knockdown (KD) HeLa cells. Mean ratio is normalized to CTR (3 experiments are shown for sh1, sh3, and sh4; 4 experiments for sh2 and sh5 ± SEM). sh1–sh5 represent different oligonucleotides used for shRNA interference; an EV is used for CTR (*p = 0.047, **p = 0.007). Molecular markers are shown on the left.

(B) Growth curves of CTR and f KD (sh2 and sh5) HeLa cells. Cells are detached and counted every 24 h. Data are mean of 3 independent experiments ± SEM.

(C) Western blot of CTR and f KD (sh2 and sh5) cell lysates recognizing the subunits of the F_1 and Fo sectors of ATP synthase and the enzyme interactors IF1 and CyPD (left panel). CS is shown as a loading control. Relative mean ratio (mean of at least 6 independent experiments ± SEM) between subunit/inhibitor and CS band pixels is shown in the right panel (*p = 0.011, **p = 0.006). Molecular markers are shown on the left.

(D) Maximal and oligomycin-inhibited (2 μM oligomycin) ATPase activities are shown as percentage of CTR. ATP hydrolysis is determined spectrophotometrically at 340 nm in permeabilized CTR or f KD (sh2 and sh5) HeLa cells (2×10^6 cells in 1 mL of ATP-regenerating system) at 37°C in the presence of 10 μM alamethicin and 10 μM decavanadate. Values are mean of 6 or 3 experiments run in triplicate ± SEM in the absence (−) or presence (+) of oligomycin, respectively.

(E) Oxygen consumption rate (OCR) of CTR and f subunit KD (sh2 and sh5) HeLa cells. OCR is measured before (basal) or after treatment with oligomycin (Oligo), carbonyl cyanide p-(trifluoromethoxy) phenylhydrazone (FCCP), rotenone (Rot), and antimycin A (AA). Left panel: representative OCR measurements of adherent cells *in situ*, seeded at a concentration of 50,000 cell/well. Right panel: mean OCR, expressed per microgram of protein content, of 3 independent experiments ± SEM.

(F) Western blot for OXPHOS complex subunits, the f subunit of ATP synthase, and prohibitin (loading control) in CTR and f KD (sh2 and sh5) mitochondria. The molecular size of each subunit is indicated on the left. Right: the mean ratio between each complex and prohibitin band pixels is normalized to CTR (3 independent experiments ± SEM).

(G) Nonyl acridine orange (NAO; 200 μM) staining quantification (fluorescence, arbitrary units) in CTR and sh2 and sh5 f KD cells (4 independent experiments ± SEM).

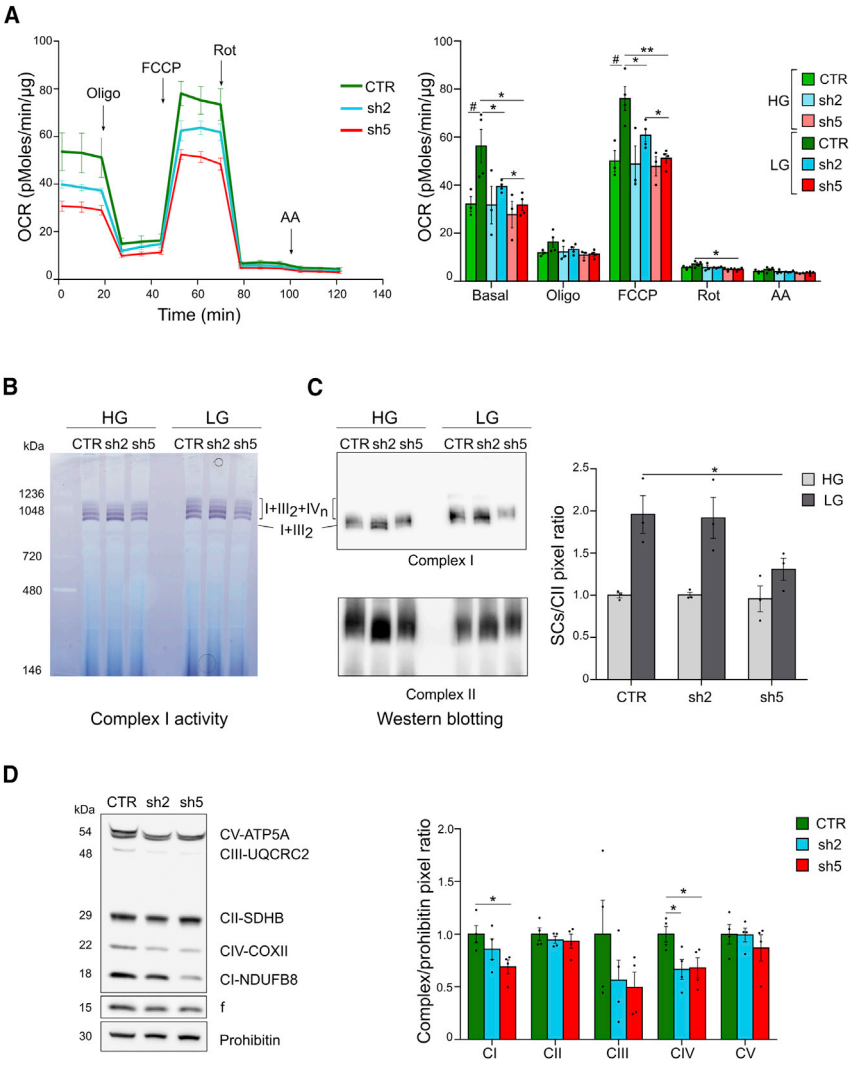

Figure 2. f subunit KD limits respiration and respiratory supercomplex assembly in low-glucose-containing medium

(A) OCR of CTR and f subunit KD (sh2 and sh5) HeLa cells grown in 2.5 mM (left and right panels) or 25 mM (right panel) glucose-containing medium for 24 h. OCR is measured before or after treatment as in Figure 1E. Left panel: representative OCR measurements of adherent cells *in situ*, seeded at a concentration of 50,000 cell/well. Right panel: mean OCR expressed per microgram of protein content of 4 independent experiments in 2.5 mM glucose medium (LG) ± SEM (*p ≤ 0.05, **p = 0.0034) compared with mean OCR per microgram of protein shown in Figure 1E and assessed in 25 mM glucose medium (HG) (#p ≤ 0.05).

(B) BN-PAGE of mitochondrial extracts obtained with 1% (w/v) digitonin concentration from CTR and sh2 and sh5 f KD HeLa cells grown in HG or LG medium for 24 h. BN-PAGE gel is stained by complex I in gel activity staining (complex I activity) and is representative of 3 independent experiments. Complex I-containing supercomplexes are indicated as $I+III_2$ and $I+III_2+IV_n$.

(C) Western blot for the Ndufs1 complex I subunit (top panel) or SDHA complex II subunit (bottom panel) of CTR, sh2, and sh5 samples obtained as in (B), representative of 3 independent experiments. Mean ratio (right panel) between complex I-containing supercomplexes (SCs) and CII band pixels of 3 independent experiments ± SEM is shown for CTR and sh2 and sh5 f KD HeLa cells grown in HG or LG medium (*p = 0.045).

(D) Western blot for OXPHOS complex subunits, the f subunit of ATP synthase, and prohibitin (loading control) in CTR and f KD (sh2 and sh5) HeLa cells grown in LG medium for 24 h. The molecular size of each subunit is indicated on the left. Right: the mean ratio between each complex subunit and prohibitin band pixels of 4 independent experiments ± SEM is normalized to CTR (*p ≤ 0.05).

(CyPD), a known sensitizer of PTP (Giorgio et al., 2010) that interacts with ATP synthase, modulating its activity (Giorgio et al., 2009), were unaffected by f subunit downregulation (Figure 1C). Considering the localization of the f subunit in the Fo sector, we tested whether downregulation of this subunit affects maximal ATPase activity. Indeed, sh2 and sh5 cells did not show changes in maximal ATP hydrolysis (Figure 1D), according to the unaltered levels of IF1 or CyPD (Figure 1C). In sh2, sh5, and control cells, the oligomycin sensitivity was around 98%. Importantly, the a and c subunit levels were not altered in sh2 or sh5 mitochondria, in line with the fact that these cells maintained their oligomycin sensitivity (Figure 1D).

When HeLa cells were grown in complete, high-glucose-containing DMEM (HG), knockdown of the f subunit did not affect mitochondrial respiration (OCR [oxygen consumption rate]) under basal, oligomycin-sensitive, and uncoupled conditions (Figure 1E). In line with unaltered respiration, HeLa sh2 or sh5 mitochondria did not show changes in the levels of OXPHOS components or in the number of mitochondria, as revealed by western blotting (Figure 1F) and nonyl acridine orange (NAO) staining (Figure 1G), respectively.

Knocking down the f subunit affects respiration and respiratory supercomplex assembly in low-glucose medium

When HeLa cells were grown for 24 h in low-glucose-containing DMEM (LG), a condition that stimulates the OCR in controls (compare LG and HG in Figure 2A, right panel), mitochondrial respiration in sh2 and sh5 f knockdown (KD) cells did not reach the levels of controls under basal or carbonyl cyanide p-(trifluoromethoxy) phenylhydrazone (FCCP)-stimulated conditions (Figure 2A). The protein levels of transporters that might affect the availability of substrates were analyzed as a possible mechanism limiting respiration in f KD cells. Indeed, glutaminase 1 (GLS1), the rate-limiting enzyme for availability of glutamate to support the Krebs cycle; the adenine nucleotide transporter (ANT3); and the pyruvate carrier (MPC1) were unchanged upon f subunit downregulation in LG medium (Figure S1A).

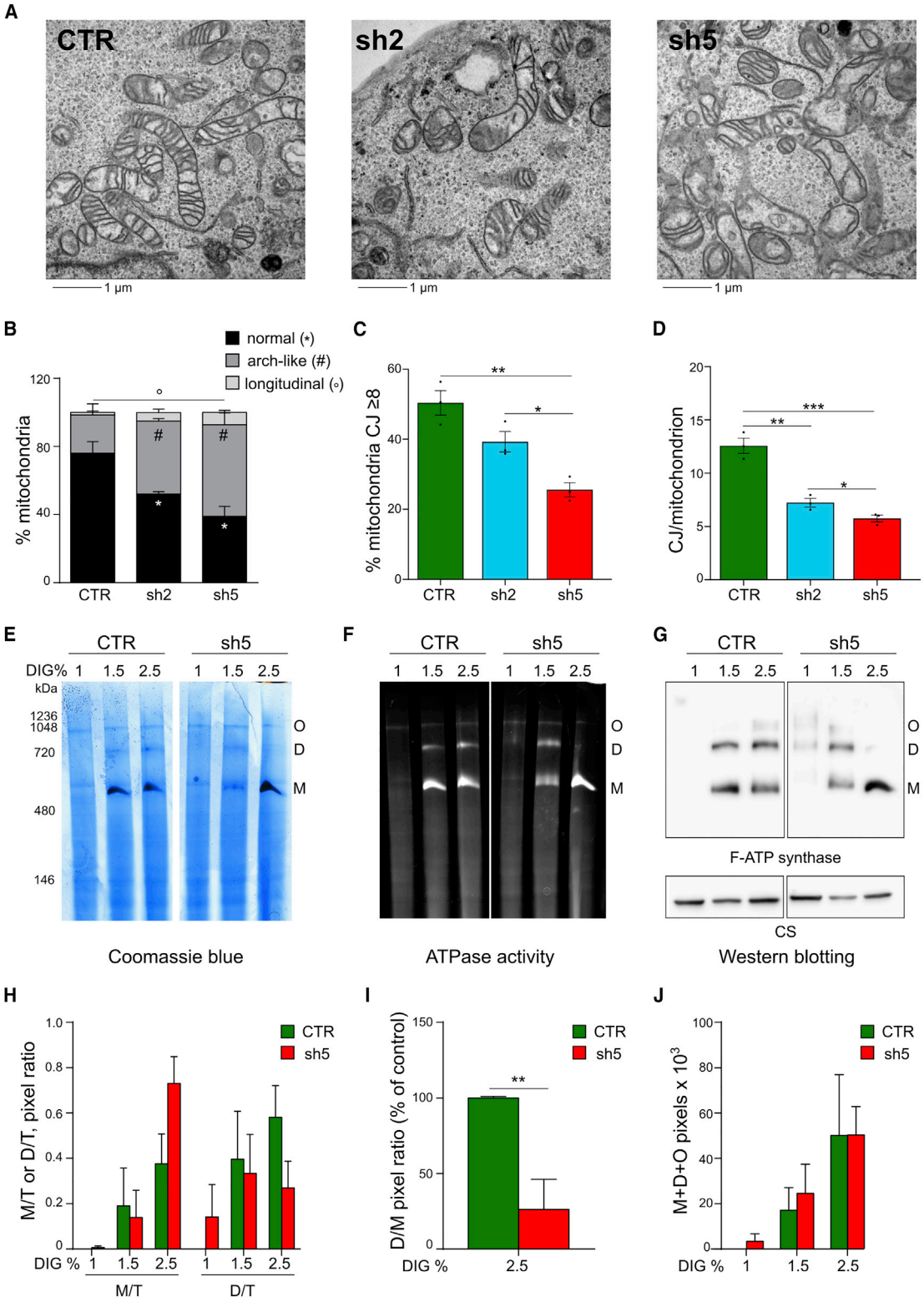

(legend on next page)

To further clarify the mechanism responsible for differences in HG or LG medium, respiratory supercomplexes were analyzed under these two conditions. Their quantification was performed by monitoring complex I, an essential component of supercomplex assembly in mammals (Lobo-Jarne and Ugalde, 2018). In control cells, supercomplexes were doubled when cells were grown in LG medium, as revealed by in-gel complex I activity staining and western blotting (Figures 2B and 2C). This did not occur in sh5 mitochondria, in which the amount of supercomplexes was significantly lower in LG medium (Figure 2C), matching the absence of an increase in respiration (Figure 2A). In sh2 mitochondria, a 30% decrease in f subunit level correlated with intermediate respiratory behavior between control and sh5 cells and a mild difference in supercomplex assembly compared with controls. Under the LG condition, western blotting analysis of OXPHOS complexes showed lower levels of complexes I and IV in sh5 f KD in comparison with control lysates (Figure 2D), a result that is also in line with lower supercomplex assembly (Figures 2B and 2C). These findings are in agreement with previous studies demonstrating the role of supercomplex formation in favoring efficient respiration (Lapuente-Brun et al., 2013) and dependence on the cellular metabolic requirement (Balsa et al., 2019; Lapuente-Brun et al., 2013).

Knocking down the f subunit alters mitochondrial crista morphology and ATP synthase dimer stability

Because respiratory supercomplex stability is determined by mitochondrial ultrastructure (Cogliati et al., 2013), we investigated mitochondrial crista morphology in f KD HeLa cells. A decreased number of cristae was observed in sh2 and sh5 mitochondria (Figure 3A). Cristae were organized in a more curved structure, described as ''arch-like,'' or in a different orientation along the major mitochondrial axis, called ''longitudinal'' (Figure 3A), as reported previously in the e/g KD HeLa cells (Habersetzer et al., 2013). The number of mitochondria characterized by these arch-like and longitudinal structures increased by decreasing the f subunit level (Figure 3B). The arbitrary threshold of 8 crista junctions (CJs; crista contacts with the outer membrane; Zick et al., 2009) per mitochondrion was defined here to objectively quantify mitochondria displaying normal morphology (Figure 3C). The f subunit levels correlate with the number of mitochondria displaying 8 more CJs (Figure 3C). Quantification indicated a significant decrease in CJs per mitochondrion in sh2 and sh5 HeLa cells (Figure 3D). Because ATP synthase dimers are crucial for crista morphology (Davies et al., 2012; Habersetzer et al., 2013), we investigated a possible role of the f subunit in dimer stability. Mitochondrial native complexes from control or sh5 f KD HeLa cells were extracted using digitonin titration and separated by blue native polyacrylamide-gel electrophoresis (BN-PAGE). ATP synthase monomers, dimers, or oligomers were identified by Coomassie staining, in-gel ATPase activity, and western blotting for the β subunit (Figures 3E–3G, respectively). Dimers and oligomers were extracted in sh5 mitochondria at 1% (w/v) digitonin but not in controls. ATP synthase dimers were less stable in sh5 than in control cells in the presence of 2.5% (w/v) digitonin (Figures 3H and 3I), suggesting that the f subunit is important in ATP synthase dimer stability. The dimer/monomer ratio was decreased significantly in sh5 at 2.5% (w/v) digitonin (Figure 3I), a fact which was not due to different detergent efficacy, as revealed by the sum of all ATP synthase species (monomers, dimers, and oligomers) extracted in each cell type (Figure 3J).

Dimers participate in formation of mitochondrial contact site and cristae organizing system (MICOS) complexes at the level of CJs (Eydt et al., 2017). To study whether downregulation of the f subunit alters mitochondrial crista architecture directly by affecting ATP synthase dimer stability or indirectly by causing MICOS complex disruption, we analyzed several MICOS components by western blotting. In f KD lysates, the amounts of mic60, mic27, mic19, and mic10 components were not significantly different compared with controls (Figure S1B), indicating that downregulation of the f subunit does not affect MICOS protein expression or degradation. Moreover, unaltered levels of mic10 and mic60 components controlling the holo-complex (Stephan et al., 2020) suggest that MICOS assembly is likely unaffected in f KD cells. Thus, it is plausible that the altered crista

Figure 3. f subunit KD in HeLa cells alters mitochondrial crista morphology and destabilizes ATP synthase dimers

(A) Representative transmission electron microscopy images of CTR and sh2 and sh5 f KD fixed HeLa cells. Mitochondrial morphology is shown. Scale bar, 1 μm.

(B) Histogram representing the number of mitochondria containing at least one arch-like or longitudinal crista. Mitochondria that do not contain these alterations are considered normal. Mitochondrial classes are quantified and expressed in percent of their total number per cell genotype ± SEM (3 independent experiments are analyzed, 10 images each experiment per condition; *, °, #$p \leq 0.05$).

(C) Histogram representing the number of mitochondria containing at least 8 crista junctions (CJs ≥ 8), expressed in percent of their total number per condition ± SEM (3 independent experiments are analyzed, 10 images each experiment per condition; *p = 0.0182, **p = 0.0036).

(D) Histogram representing the mean number of CJs per mitochondrion ± SEM (3 independent experiments are analyzed, 5 images each experiment per condition; *p = 0.043, **p = 0.0029, ***p = 0.0009).

(E) BN-PAGE of mitochondrial extracts obtained with the indicated digitonin concentrations (DIG %, w/v) from CTR and sh5 f KD HeLa cells. The gel is subjected to Coomassie blue staining. The image is representative of 3 independent experiments.

(F) Oligomers (O), dimers (D), and monomers (M) of ATP synthase, extracted as in (E), are identified by ATPase in-gel activity staining (ATPase activity). The image is representative of 3 independent experiments.

(G) Western blot for the β subunit of the BN-PAGE gel obtained as in (E) and transferred to a polyvinylidene fluoride (PVDF) membrane. Os, Ds, and Ms of ATP synthase containing the β subunit are indicated on the right. CS is shown as a loading control. The image is representative of 3 independent experiments.

(H) The mean pixel ratio between Ms or Ds and the total ATP synthase extract (T) detected by western blotting (as in G) is shown for each DIG condition (DIG %, w/v) in CTR and sh5 f KD HeLa mitochondrial extracts. Data are mean of 3 experiments ± SEM.

(I) The mean pixel ratio between bands of extracted ATP synthase Ds and Ms (D/M) in CTR and sh5 f KD HeLa mitochondrial extracts (in G) is shown. Data are mean of 4 experiments presented as percentage of CTR ± SEM (**p = 0.014).

(J) Total pixels derived from the sum of Ms, Ds, and Os of ATP synthase (in G) are shown at the indicated DIG concentrations (DIG %, w/v) for CTR and sh5 f KD mitochondrial extracts. Data are mean of 3 experiments ± SEM.

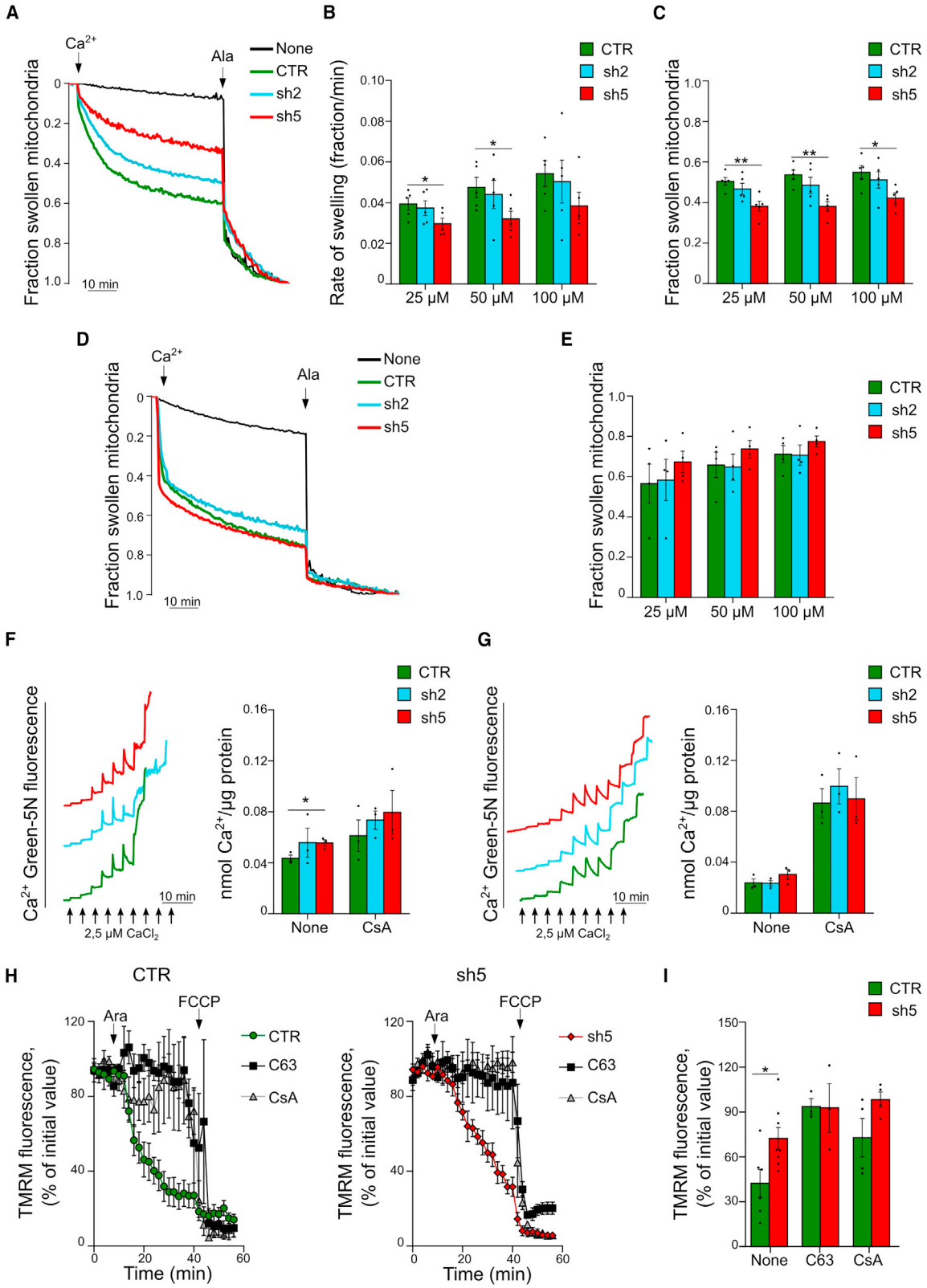

(legend on next page)

morphology in f KD cells is due to ATP synthase dimer instability per se.

The f subunit affects PTP size and its sensitivity to calcium and arachidonic acid

Given the role of the f subunit in ATP synthase dimer stability, its involvement in PTP modulation was investigated. Importantly, downregulation of the f subunit does not affect enzyme subunit stoichiometry or respiration in HG medium, allowing us to study its effect on PTP modulation without the effects of lack of other subunits or differences in calcium uptake or mitochondrial membrane potential. We analyzed PTP-dependent swelling in mitochondria derived from sh2, sh5, and control HeLa cells. In sucrose-based medium, molecules with a 4.4-Å radius (Massari and Azzone 1972), when hydrated, can diffuse only through the largest channels. PTP opening was triggered by Ca^{2+} addition of 50 μM (Figure 4A) or 25–100 μM (Figures 4B and 4C). The rate of swelling because of sucrose diffusion and the fraction of swollen mitochondria were lower in sh5 and sh2 than in control mitochondria (Figures 4B and 4C), resembling the f subunit downregulation level. In f KD cells, the population of mitochondria was heterogeneous. One fraction did not allow sucrose diffusion, whereas another fraction did; the latter being represented by swollen mitochondria (Figure 4C). A possible explanation might be that the fraction of sh2 and sh5 swollen mitochondria properly forms channels of a large size in the presence of remaining f subunit. However, this hypothesis remains to be verified because of the limitation of this method, which does not allow monitoring individual organelles. In KCl-based medium (radius below 2 Å in K^+ and Cl^- ions; Heyrovská 1989), the rate of swelling is fast, and solute diffusion can take place in channels of small and large sizes. The fraction of swollen mitochondria in sh2 and sh5 cells did not differ from that of controls (Figures 4D and 4E). It indicates that decreased levels of the f subunit do not prevent opening of the PTP and diffusion of small-size solutes. Moreover, induction of maximal possible swelling by alamethicin (Figures 4A and 4D), which was comparable in f KD and control phenotypes, indicates that the differences (Figure 4A) are due to PTP size.

To further analyze channel size, we studied mitochondrial swelling of sh5 and control cells (Figures S1C and S1D) in solutions of equivalent osmotic pressure and containing arabinose or polyethylene glycol (PEG) of increasing molecular size up to 1,500 Da (Carroll et al., 2019; Massari and Azzone, 1972; Pfeiffer et al., 1995). Fractions of swollen mitochondria in PEG solution of 200 Da were decreased significantly in sh5 cells, confirming a smaller PTP size in f KD cells (Figure S1D). Differences between sh5 and control cells became gradually less evident in solutions containing PEG of higher molecular weight because of the decrease in the fraction of swollen control mitochondria up to 1,500 Da PEG, the condition under which mitochondria of neither cell type were able to swell (Figures S1C and S1D).

The calcium retention capacity assay showed that the Ca^{2+} sensitivity of PTP was decreased in sh5 cells (Figures 4F and 4G), with a significant difference in sucrose-based medium (Figure 4F), whereas inhibition by cyclosporine A (CsA) was observed independently of the cell genotypes. However, it cannot be excluded that PTP desensitization to Ca^{2+} in f KD cells is due to altered mitochondrial morphology, given that different crista organization in pre-swollen organelles desensitizes PTP opening to Ca^{2+} (Baev et al., 2018).

We further tested the effect of arachidonic acid, which sensitizes PTP to opening (Scorrano et al., 2001). Mitochondrial depolarization caused by PTP opening was followed, upon addition of

Figure 4. f subunit KD decreases the size of the PTP and its sensitivity to calcium or arachidonic acid in HeLa cells

(A) Swelling of mitochondria isolated from CTR and sh2 and sh5 f KD HeLa cells is assayed in sucrose- based medium and measured as a decrease in absorbance at 540 nm. Where indicated, 50 μM Ca^{2+} and 1 μM alamethicin (Ala) are added. The fraction of swollen mitochondria after PTP opening is calculated and normalized to the maximal swelling induced by Ala (referred to as 1). Traces are representative of 5 independent experiments.

(B) The histogram refers to the mean rate of swelling (fraction of swollen mitochondria/minute) in sucrose medium ± SEM. The rate of swelling is measured during the first 5 min of PTP opening by calculation of the slope of the tangent line per trace of swelling. Data are mean of 5 independent experiments for each Ca^{2+} concentration (*$p < 0.05$).

(C) The histogram refers to the mean fraction ± SEM of swollen mitochondria in sucrose medium after Ca^{2+} addition (0–100 μM), at defined time points, as reported in STAR Methods. Mean of 5 independent experiments for each Ca^{2+} concentration is shown (*$p = 0.015$, **$p < 0.001$).

(D) Swelling of mitochondria isolated from CTR and sh2 and sh5 f KD HeLa cells is assayed in KCl-based medium and measured as a decrease in absorbance at 540 nm. Where indicated, 50 μM Ca^{2+} and 1 μM Ala are added. The fraction of swollen mitochondria after PTP opening is calculated and normalized to the maximal swelling induced by Ala (referred to as 1). Traces are representative of 4 independent experiments.

(E) The histogram refers to the mean fraction ± SEM of swollen mitochondria in KCl medium after Ca^{2+} addition (0–100 μM) at defined time points, as reported in STAR Methods. Mean of 4 independent experiments for each Ca^{2+} concentration is shown.

(F and G) Ca^{2+} retention capacity (CRC) is assessed in permeabilized CTR and sh2 and sh5 f KD HeLa cells in sucrose-based (F) or KCl-based (G) medium containing respiratory substrates and the membrane-impermeable Ca^{2+} sensor Ca^{2+} Green-5N. Ca^{2+} Green-5N fluorescence was monitored following repeated addition of Ca^{2+} pulses. A return of Ca^{2+} Green-5N fluorescence to baseline reflects uptake of Ca^{2+} by mitochondria, whereas a sudden increase in fluorescence is indicative of PTP opening. One experiment representative of 3 is shown in the left panels. Ca^{2+} Green-5N fluorescence baselines are graphically shifted upward to avoid trace overlap. Right panels: the histogram represents nanomoles of Ca^{2+} per microgram of protein retained by CTR (green bars), sh2 (blue bars), and sh5 (red bars) cells under basal conditions (none) or in the presence of 1.6 μM cyclosporin A (CsA). Data represent the mean ± SEM (3 independent experiments run in triplicate each condition; *$p = 0.029$).

(H) Mitochondrial membrane potential (TMRM) was monitored in CTR or sh5 f KD (sh5) HeLa cells. To inhibit PTP, cells were incubated with 3.2 μM CsA or 1 μM of compound 63 (C63) for 30 min before TMRM measurements. Where indicated, 8 μM arachidonic acid (Ara) and 5 μM FCCP were added. Fluorescence is expressed as percentage of the initial values for the condition. Traces are mean ± SEM of 6 or 8 experiments for untreated CTR or sh5 cells, respectively; 3 experiments for C63- and 4 for CsA-treated cells.

(I) The histogram represents the mean TMRM fluorescence, expressed as percent of initial values ± SEM, 24 min after addition of Ara in the absence (none; mean ± SEM of 6 or 8 experiments for CTR or sh5, respectively; *$p = 0.024$) or presence of CsA (mean ± SEM of 4 experiments for CTR and sh5) or C63 (mean ± SEM of 3 experiments for CTR and sh5).

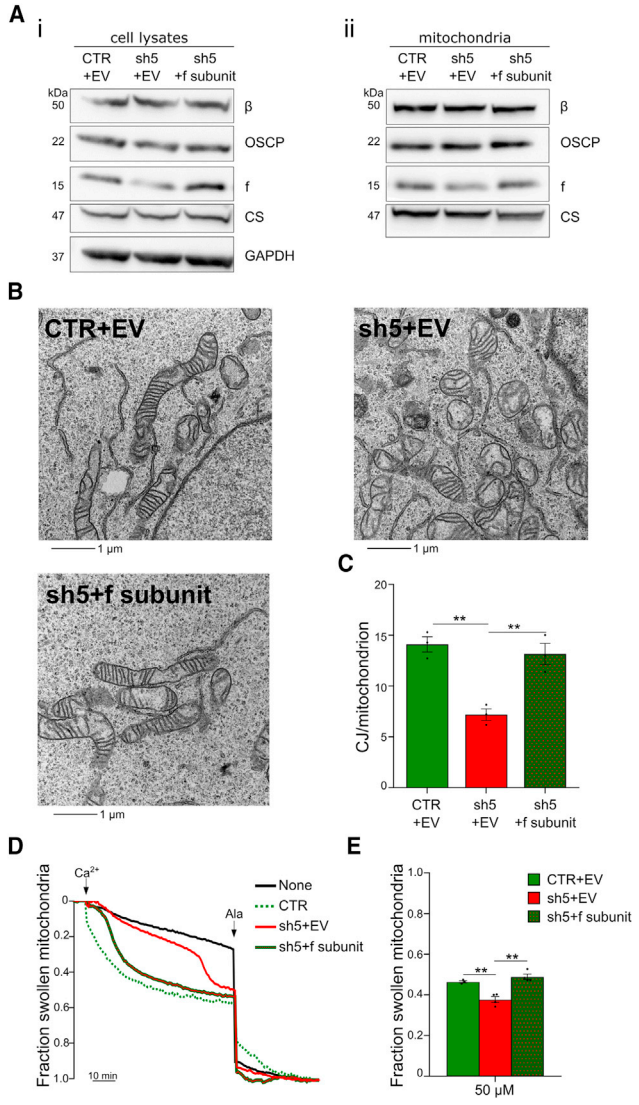

Figure 5. f subunit re-expression in sh5 f KD HeLa cells rescues mitochondrial crista morphology and PTP-dependent swelling

(A) Western blot of (i) total cell lysates or (ii) isolated mitochondria in CTR (CTR+EV), f KD (sh5+EV), and f KD re-expressing the f subunit (sh5+f subunit) HeLa cells, transiently transfected. To rescue f subunit expression, HeLa sh5 f KD cells were transfected with a pcDNA3.1 vector containing a shRNA5-resistant *ATP5J2* pcDNA (sh5+f subunit). The pcDNA3.1 empty vector (EV) was used to generate proper experimental CTRs (CTR+EV and sh5+EV). CS, GAPDH, and the ATP synthase subunits f, OSCP, and β are detected. Molecular markers are shown on the left.

(B) Representative transmission electron microscopy images of CTR+EV, sh5+EV, and sh5+f subunit fixed HeLa cells, obtained as in (A). Mitochondrial morphology is shown. Scale bar, 1 μm.

(C) The histogram represents the mean number of CJs per mitochondrion ± SEM (3 independent experiments are analyzed, 5 images each experiment per condition; **$p < 0.001$).

(D) Swelling of mitochondria isolated from sh5+EV and sh5+f subunit HeLa cells is assayed in sucrose-based medium and measured as a decrease of absorbance at 540 nm, as in Figure 4A. As a reference to previous swelling experiments, the fraction of swollen mitochondria in CTR HeLa cells (as in Figure 4A) is shown as a dashed trace. Where indicated, 50 μM Ca^{2+} and 1 μM Ala are added. The fraction of swollen mitochondria after PTP opening is calculated and normalized to the maximal swelling induced by Ala (referred to as 1). Traces are representative of at least 4 independent experiments.

(E) The histogram refers to the mean fraction ± SEM of swollen mitochondria from CTR+EV, sh5+EV, and sh5+f subunit HeLa cells in sucrose-based medium after 50 μM Ca^{2+} addition at defined time points, as reported in STAR Methods. Mean of 3 independent experiments for CTR+EV and 4 experiments for sh5+EV and sh5+f subunit is shown (**$p < 0.001$).

arachidonic acid to control and sh5 f KD cells, by monitoring their tetramethylrhodamine methyl ester (TMRM) fluorescence (Figure 4H). Loss of membrane potential upon arachidonic acid treatment was prevented by CsA (Broekemeier et al., 1989) and by a 5-chloro-2-methylphenylanilino analog called compound 63 (Roy et al., 2015), another potent inhibitor of the channel (Figures 4H and 4I), confirming the specific effect of arachidonic acid on PTP opening. Titration of arachidonic acid was performed to define the lowest effective dose causing PTP opening (Figures S1E and S1F). Importantly, arachidonic acid-dependent depolarization was delayed in sh5 f KD cells (Figures 4H and 4I), suggesting resistance to PTP opening *in situ*. Mitochondria of f KD cells were completely depolarized in the presence of FCCP, in line with a normal response of their membrane potential to stimuli. These findings suggest that the f subunit controls the size and sensitivity of the Ca^{2+}-dependent channel.

Re-expression of the f subunit rescues mitochondrial crista morphology and PTP-dependent swelling

Reintroduction of the f subunit in sh5 f KD cells was achieved through transient transfection with a pcDNA 3.1 vector containing a shRNA-resistant f subunit sequence. The endogenous immature f subunit does not possess the mitochondrial targeting sequence, unlike the other ATP synthase subunits. Instead, its mitochondrial import is a PKA-dependent process that involves binding of a structural motif in the f subunit 3′ UTR to the mitochondrial AKAP121 protein (Feliciello et al., 2005; Ginsberg et al., 2003). To overcome possible limitations in import of the f subunit, the f sequence was preceded in the expression vector by the mitochondrial targeting sequence found in mammalian cytochrome *c* oxidase subunit VIII (Rizzuto et al., 1992). Subunits β and OSCP were identical in control and sh5 f KD cells carrying the empty vector and in sh5 cells re-expressing the f subunit (Figure 5A, left). Moreover, western blotting analysis of isolated mitochondria confirmed that the f subunit was targeted properly to the organelles (Figure 5A, right). Indeed, the mitochondrial morphology and CJs per mitochondrion of cells re-expressing the f subunit appeared to be identical to that in control cells and ameliorated compared with the sh5 f KD phenotype (Figures 5B and 5C), confirming a crucial role of this subunit in keeping normal mitochondrial morphology.

PTP-dependent swelling in sucrose-based medium was measured upon f subunit rescue in sh5 f KD HeLa cells. The rate of swelling and the fraction of swollen mitochondria in cells re-expressing the f subunit became similar to that in control cells (Figure 5D), allowing diffusion of sucrose molecules. Sucrose molecules were instead excluded in sh5 f KD cells transfected with an empty vector and characterized by channels of smaller size (Figures 5D and 5E). The massive mitochondrial swelling in cells re-expressing the f subunit (sh5+f subunit), but not in their

counterpart lacking the protein (sh5 + empty vector [EV]), strongly suggests the importance of this subunit in formation of the channel and modulation of its size.

DISCUSSION

These results demonstrate that the human f subunit of ATP synthase is essential for dimer stability, normal mitochondrial crista morphology, and modulation of PTP opening. Downregulation of this subunit up to 70% does not affect ATP synthase catalytic activity in complete medium, highlighting that PT and catalysis are separate functions of the same enzyme.

This study aims to characterize the f subunit physiological role(s) by its downregulation in HeLa cells. This human model was conceived to overcome the bioenergetics alterations that were found in haploid human cells depleted of the f subunit (HAP1-Δf cells) (He et al., 2018; Carroll et al., 2019). These f-null clones show a milder phenotype compared with the lack of survival described for the f-null yeast strain (Spannagel et al., 1997); nevertheless, they are characterized by a decrease in mitochondrial function and changes in the respiratory complexes (He et al., 2018). Moreover, HAP1-Δf clones do not show oligomycin-sensitive respiration according to alteration of the amount of the a subunit and display dimer instability and downregulation of the other Fo subunits A6L, diabetes-associated protein in insulin-sensitive tissue (DAPIT), and 6.8PL (He et al., 2018). Whether, in these f-null HAP1 cells, the effect on dimer stability was due to the lack of the f subunit or the decrease of the other Fo components still remains to be clarified.

We generated two populations of HeLa cells in which the f subunit level remained at 70% (sh2) or 30% (sh5). KD of the f subunit did not alter ATP synthase subunit composition, mitochondrial respiration, or respiratory chain content in HG medium. ATP synthase monomers were fully assembled, and no "vestigial" forms were revealed as they were instead seen in HAP1-Δf cells. This difference in monomer stability might be explained by the fact that *ATP5J2* gene disruption decreases transcription (or assembly) of other subunits, as observed in the f-null HAP1 clones. Indeed, Fo-Fo dimers were destabilized by the decrease in the f subunit in our sh5 model treated with detergent, highlighting the importance of this subunit in ATP synthase dimerization.

Unexpectedly, dimer destabilization did not affect enzyme coupling or its catalytic activity. Purified yeast monomers lacking the dimer-specific e, g, and k subunits displayed ATPase activity similar to dimers containing those subunits (Hahn et al., 2016), suggesting that detergent treatment might affect regulatory mechanisms that are present in intact mitochondria. Similarly, the lack of effect on the ATPase activity observed in our f KD cells may be a consequence of HeLa cell permeabilization. However, it is plausible that downregulation of the f subunit does not affect ATPase activity and oligomycin sensitivity, considering that the interactions between the f and a subunits involve residues that are far from the region where the a and c subunits interact (Spikes et al., 2020). ATP synthesis was also unaffected in f KD cells growing in HG medium, suggesting that the contacts and conformation of the long horizontal helices in the a subunit, which are involved in proton-coupled ATP synthesis (Kühlbrandt and Davies, 2016), are probably unaffected by downregulation of the f subunit. Alternatively, the residual f subunit might be sufficient to maintain 30% of the normal mitochondrial population, a threshold shown to be adequate to sustain efficient mitochondrial function (Nuskova et al., 2020), even in mitochondrial diseases (Chomyn et al., 1992; Taylor and Turnbull, 2005).

The latest hypothesis is in line with our observation that, in LG medium, a condition that stimulates respiration in control cells, the OCR levels of f KD cells were not increased compared with the HG condition. This fact is supported by limited OXPHOS supercomplex formation in f KD cells displaying abnormal cristae, as reported previously in other models (Lobo-Jarne and Ugalde, 2018).

In f KD HeLa populations, the number of CJs was reduced significantly, and the crista shape recalled the arch-like structures and longitudinal orientation described previously for HeLa cells depleted of the e or g subunit (Habersetzer et al., 2013). These previous results, together with our findings, indicate that these crista rearrangements are due to dimer instability (or their altered conformation) but not associated specifically with any of the Fo subunits (f, g, or e) or to depletion of the OXPHOS complexes Mfn1 or Opa1, as suggested by Habersetzer et al. (2013). ATP synthase dimers are important for crista curvature (Davies et al., 2012) and involved in formation of MICOS complexes at the level of the CJ (Eydt et al., 2017). These complexes establish an inner membrane architecture (Friedman et al., 2015). It has been shown that the e subunit of ATP synthase is involved in the interaction with Mic10, a MICOS component (Eydt et al., 2017). Because f subunit downregulation causes dimer instability, we assessed MICOS components required for proper CJ formation in f KD cells. Unaltered levels of MICOS proteins in f KD cells suggest the presence of holocomplexes because it has been shown that expressed MICOS components are assembled into the complex when mic60 and mic10 are present (Stephan et al., 2020). Therefore, the arch-like or longitudinal crista morphology observed in f KD cells is mainly due to ATP synthase dimer instability. The f subunit re-expression in f KD cells rescued mitochondrial morphology, pointing to a crucial role of the f subunit in dimer stability and crista organization. Although highly unlikely, indirect involvement of MICOS complexes in crista organization cannot be entirely excluded. Future studies focusing on the interplay between the f subunit and MICOS assembly will address this issue.

The impaired respiratory supercomplex assembly in LG medium shows that downregulation of the f subunit have deleterious consequences under conditions requiring high mitochondrial activity to meet the energy demand.

Downregulation of the f subunit also affected the size and Ca^{2+} sensitivity of the PTP in HeLa cells. These findings support the idea that ATP synthase becomes the PTP upon conformational changes in the Fo sector (Alavian et al., 2014; Giorgio et al., 2013; Mnatsakanyan et al., 2019; Urbani et al., 2019). Our working hypothesis is that Ca^{2+} binding to the catalytic F_1 leads to opening of a latent megachannel in the Fo, following structural changes that might be conducted through the peripheral stalk (Giorgio et al., 2018, 2017). The yeast e, g, and b subunits modulate the size of the Ca^{2+}-activated channel (Carraro et al., 2018; Guo et al., 2019). There are independent studies of HeLa and

HAP1 cells supporting the hypothesis that the Fo sector might be the site where PT occurs (Alavian et al., 2014; Neginskaya et al., 2019). However, in human models, ablation of the c, e, g, and b subunits also affects mitochondrial function as a whole and the levels of other ATP synthase subunits (He et al., 2017a, 2017b, 2018) making the PTP studies unreliable. Carroll et al. (2019) noticed that, in f-null HAP1 cells, PTP opening does occur, measured as mitochondrial swelling. However, the rate of mitochondrial swelling of these HAP-1 clones was decreased compared with their controls. This finding is in line with a reduced swelling rate measured in our f KD HeLa models and indicates that PTP size is decreased upon f subunit downregulation. Although it remains to be established whether the smaller channel observed in f KD mitochondria might be formed by ANT, as reported for the c subunit knockout (KO) model (Neginskaya et al., 2019), involvement of the f subunit in the PT large conductance channel has been established here. Indeed, the re-expression of the f subunit in f KD cells rescued sucrose diffusion upon PTP opening to the extent of controls, highlighting the importance of the f subunit in formation of large channels.

Taking advantage of the available cryo-EM studies in *S. cerevisiae* (PDB: 6B2Z; Guo et al., 2017) and *B. taurus* (PDB: 6ZBB; Spikes et al., 2020) it is possible to predict the human f subunit topology and the aminoacidic residues that might be involved in the interaction with neighboring subunits responsible for dimer stability. In the yeast structures, residues in the C terminus of the f subunit form a number of hydrophobic interactions with the two a subunits, each belonging to a monomeric Fo (indicated as a or a' in Figure S2A, right panel), highly conserved in the human sequence (Figure S2C). These interactions suggest that the f subunit may play a role in keeping the a-a' dimer in close contact. Downstream of the aforementioned part of the f subunit is the hydrophilic C-terminal end, which has been resolved only recently in the bovine enzyme and contacts subunits a, b, e, and g (Figure S2B), imposing a 3.0-Å cutoff distance. Homology prediction of the 3D structure of the human f subunit suggests that its conformation is similar to that observed in yeast in the region limited by amino acids 64–83 (PDB: 6B2Z; Figure S2D). The mammalian structures (Gu et al., 2019; Pinke et al., 2020; Spikes et al., 2020) are conserved and support the hypothesis of high motility of the f subunit because of the presence of lipids (Spikes et al., 2020). Overall sequence analysis and homology prediction support a possible role of the f subunit in keeping dimer stability and in PTP modulation.

We demonstrated here that one human subunit in the Fo region of ATP synthase is involved in the channel structure without affecting enzyme catalysis. Indeed, downregulation of the f subunit decreases, and its re-expression rescues, the channel size. Furthermore, the decreased Ca^{2+} sensitivity of the f KD PTPs provides a piece of evidence toward our working hypothesis that the Ca^{2+}-induced conformational changes (Giorgio et al., 2018, 2017) are transmitted to the Fo. The f subunit, which is part of the peripheral stalk, might be an important connection to the Fo sector in transmission of signals that allow PT.

In conclusion, downregulation of the human f subunit does not alter enzyme stoichiometry or catalysis. Its key localization is fundamental for normal ATP synthase dimer stability, crista morphology, and PTP modulation, with important consequences for cell capability to respond to high bioenergetic demand and apoptotic stimuli.

STAR★METHODS

Detailed methods are provided in the online version of this paper and include the following:

- KEY RESOURCES TABLE
- RESOURCE AVAILABILITY
  - Lead contact
  - Materials availability
  - Data and code availability
- EXPERIMENTAL MODEL AND SUBJECT DETAILS
- METHODS DETAILS
  - Stable knocking down of the f subunit
  - Transient f subunit re-expression
  - Growth curve
  - Lysates, gel electrophoresis, western blotting
  - Cell permeabilization, mitochondria preparation
  - ATP hydrolysis
  - Oxygen consumption
  - Nonyl Acridine Orange staining
  - Blue native gel electrophoresis
  - Electron Microscopy
  - Mitochondrial swelling
  - Ca^{2+} retention capacity
  - Mitochondrial membrane potential
  - Structure analysis of the human f subunit
- QUANTIFICATION AND STATISTICAL ANALYSIS

SUPPLEMENTAL INFORMATION

Supplemental information can be found online at https://doi.org/10.1016/j.celrep.2021.109111.

ACKNOWLEDGMENTS

The research leading to these results has received funding from AIRC under the MFAG 2017 – ID. 20316 and MIUR under the PRIN 2017 – ID. 201789LFKB projects, P.I. V.G. We thank Diego De Stefani, Nina Kaludercic, Cristina Mammucari, Anna Raffaello, Denis Vecellio Reane, Rosario Rizzuto, Paolo Bernardi, and Ildikó Szabó for helpful suggestions. We also acknowledge the electron microscopy facility: https://www.biologia.unipd.it/servizi/servizi-alla-ricerca/servizi-dipartimentali/imaging-facility/electron-microscopy-facility/.

AUTHOR CONTRIBUTIONS

V.G. and C.G. conceived the study. V.G., G.L., and C.G. suggested experiments, C.G. and F.B. performed experiments. G.M. and S.T. conceived and performed structural and sequence analyses. C.G. performed statistical analysis. G.C., V.P., and G.L. provided critical advice. V.G. and C.G. wrote the manuscript.

DECLARATION OF INTERESTS

The authors declare no competing interests.

Received: February 24, 2020
Revised: March 11, 2021
Accepted: April 20, 2021
Published: May 11, 2021

REFERENCES

Abrahams, J.P., Leslie, A.G., Lutter, R., and Walker, J.E. (1994). Structure at 2.8 A resolution of F1-ATPase from bovine heart mitochondria. Nature *370*, 621–628.

Alavian, K.N., Beutner, G., Lazrove, E., Sacchetti, S., Park, H.A., Licznerski, P., Li, H., Nabili, P., Hockensmith, K., Graham, M., et al. (2014). An uncoupling channel within the c-subunit ring of the F1FO ATP synthase is the mitochondrial permeability transition pore. Proc. Natl. Acad. Sci. USA *111*, 10580–10585.

Antoniel, M., Jones, K., Antonucci, S., Spolaore, B., Fogolari, F., Petronilli, V., Giorgio, V., Carraro, M., Di Lisa, F., Forte, M., et al. (2018). The unique histidine in OSCP subunit of F-ATP synthase mediates inhibition of the permeability transition pore by acidic pH. EMBO Rep. *19*, 257–268.

Arselin, G., Vaillier, J., Salin, B., Schaeffer, J., Giraud, M.F., Dautant, A., Brèthes, D., and Velours, J. (2004). The modulation in subunits e and g amounts of yeast ATP synthase modifies mitochondrial cristae morphology. J. Biol. Chem. *279*, 40392–40399.

Baev, A.Y., Elustondo, P.A., Negoda, A., and Pavlov, E.V. (2018). Osmotic regulation of the mitochondrial permeability transition pore investigated by light scattering, fluorescence and electron microscopy techniques. Anal. Biochem. *552*, 38–44.

Balsa, E., Soustek, M.S., Thomas, A., Cogliati, S., García-Poyatos, C., Martín-García, E., Jedrychowski, M., Gygi, S.P., Enriquez, J.A., and Puigserver, P. (2019). ER and Nutrient Stress Promote Assembly of Respiratory Chain Supercomplexes through the PERK-eIF2α Axis. Mol. Cell *74*, 877–890.e6.

Bateman, A., Martin, M.J., O'Donovan, C., Magrane, M., Alpi, E., Antunes, R., Bely, B., Bingley, M., Bonilla, C., Britto, R., et al.; The UniProt Consortium (2017). UniProt: the universal protein knowledgebase. Nucleic Acids Res. *45* (*D1*), D158–D169.

Belogrudov, G.I., Tomich, J.M., and Hatefi, Y. (1996). Membrane topography and near-neighbor relationships of the mitochondrial ATP synthase subunits e, f, and g. J. Biol. Chem. *271*, 20340–20345.

Bernardi, P., Scorrano, L., Colonna, R., Petronilli, V., and Di Lisa, F. (1999). Mitochondria and cell death. Mechanistic aspects and methodological issues. Eur. J. Biochem. *264*, 687–701.

Bernardi, P., Rasola, A., Forte, M., and Lippe, G. (2015). The mitochondrial permeability transition pore: channel formation by F-ATP synthase, integration in signal trasduction, and role in pathophysiology. Physiol. Rev. *95*, 1111–1155.

Bienert, S., Waterhouse, A., de Beer, T.A.P., Tauriello, G., Studer, G., Bordoli, L., and Schwede, T. (2017). The SWISS-MODEL Repository-new features and functionality. Nucleic Acids Res. *45* (*D1*), D313–D319.

Bisetto, E., Di Pancrazio, F., Simula, M.P., Mavelli, I., and Lippe, G. (2007). Mammalian ATPsynthase monomer versus dimer profiled by blue native PAGE and activity stain. Electrophoresis *28*, 3178–3185.

Blum, T.B., Hahn, A., Meier, T., Davies, K.M., and Kühlbrandt, W. (2019). Dimers of mitochondrial ATP synthase induce membrane curvature and self-assemble into rows. Proc. Natl. Acad. Sci. USA *116*, 4250–4255.

Boyer, P.D. (2000). Catalytic site forms and controls in ATP synthase catalysis. Biochim. Biophys. Acta *1458*, 252–262.

Broekemeier, K.M., Dempsey, M.E., and Pfeiffer, D.R. (1989). Cyclosporin A is a potent inhibitor of the inner membrane permeability transition in liver mitochondria. J. Biol. Chem. *264*, 7826–7830.

Carraro, M., Giorgio, V., Šileikytė, J., Sartori, G., Forte, M., Lippe, G., Zoratti, M., Szabò, I., and Bernardi, P. (2014). Channel formation by yeast F-ATP synthase and the role of dimerization in the mitochondrial permeability transition. J. Biol. Chem. *289*, 15980–15985.

Carraro, M., Checchetto, V., Sartori, G., Kucharczyk, R., di Rago, J.P., Minervini, G., Franchin, C., Arrigoni, G., Giorgio, V., Petronilli, V., et al. (2018). High-conductance channel formation in yeast mitochondria is mediated by F-ATP synthase e and g subunits. Cell. Physiol. Biochem. *50*, 1840–1855.

Carroll, J., He, J., Ding, S., Fearnley, I.M., and Walker, J.E. (2019). Persistence of the permeability transition pore in human mitochondria devoid of an assembled ATP synthase. Proc. Natl. Acad. Sci. USA *116*, 12816–12821.

Chomyn, A., Martinuzzi, A., Yoneda, M., Daga, A., Hurko, O., Johns, D., Lai, S.T., Nonaka, I., Angelini, C., and Attardi, G. (1992). MELAS mutation in mtDNA binding site for transcription termination factor causes defects in protein synthesis and in respiration but no change in levels of upstream and downstream mature transcripts. Proc. Natl. Acad. Sci. USA *89*, 4221–4225.

Cogliati, S., Frezza, C., Soriano, M.E., Varanita, T., Quintana-Cabrera, R., Corrado, M., Cipolat, S., Costa, V., Casarin, A., Gomes, L.C., et al. (2013). Mitochondrial cristae shape determines respiratory chain supercomplexes assembly and respiratory efficiency. Cell *155*, 160–171.

Collinson, I.R., Runswick, M.J., Buchanan, S.K., Fearnley, I.M., Skehel, J.M., van Raaij, M.J., Griffiths, D.E., and Walker, J.E. (1994). Fo membrane domain of ATP synthase from bovine heart mitochondria: purification, subunit composition, and reconstitution with F1-ATPase. Biochemistry *33*, 7971–7978.

Daum, B., Walter, A., Horst, A., Osiewacz, H.D., and Kühlbrandt, W. (2013). Age-dependent dissociation of ATP synthase dimers and loss of inner-membrane cristae in mitochondria. Proc. Natl. Acad. Sci. USA *110*, 15301–15306.

Davies, K.M., Strauss, M., Daum, B., Kief, J.H., Osiewacz, H.D., Rycovska, A., Zickermann, V., and Kühlbrandt, W. (2011). Macromolecular organization of ATP synthase and complex I in whole mitochondria. Proc. Natl. Acad. Sci. USA *108*, 14121–14126.

Davies, K.M., Anselmi, C., Wittig, I., Faraldo-Gómez, J.D., and Kühlbrandt, W. (2012). Structure of the yeast F1Fo-ATP synthase dimer and its role in shaping the mitochondrial cristae. Proc. Natl. Acad. Sci. USA *109*, 13602–13607.

Di Pancrazio, F., Mavelli, I., Isola, M., Losano, G., Pagliaro, P., Harris, D.A., and Lippe, G. (2004). In vitro and in vivo studies of F(0)F(1)ATP synthase regulation by inhibitor protein IF(1) in goat heart. Biochim. Biophys. Acta *1659*, 52–62.

Dudkina, N.V., Sunderhaus, S., Braun, H.P., and Boekema, E.J. (2006). Characterization of dimeric ATP synthase and cristae membrane ultrastructure from Saccharomyces and Polytomella mitochondria. FEBS Lett. *580*, 3427–3432.

Dudkina, N.V., Oostergetel, G.T., Lewejohann, D., Braun, H.P., and Boekema, E.J. (2010). Row-like organization of ATP synthase in intact mitochondria determined by cryo-electron tomography. Biochim. Biophys. Acta *1797*, 272–277.

Eydt, K., Davies, K.M., Behrendt, C., Wittig, I., and Reichert, A.S. (2017). Cristae architecture is determined by an interplay of the MICOS complex and the F_1F_O ATP synthase via Mic27 and Mic10. Microb. Cell *4*, 259–272.

Feliciello, A., Gottesman, M.E., and Avvedimento, E.V. (2005). cAMP-PKA signaling to the mitochondria: protein scaffolds, mRNA and phosphatases. Cell. Signal. *17*, 279–287.

Frezza, C., Cipolat, S., and Scorrano, L. (2007). Organelle isolation: functional mitochondria from mouse liver, muscle and cultured fibroblasts. Nat. Protoc. *2*, 287–295.

Friedman, J.R., Mourier, A., Yamada, J., McCaffery, J.M., and Nunnari, J. (2015). MICOS coordinates with respiratory complexes and lipids to establish mitochondrial inner membrane architecture. eLife *4*, 1–25.

Galber, C., Valente, G., Von Stockum, S., and Giorgio, V. (2019). Purification of Functional F-ATP Synthase. Methods Mol. Biol. *1925*, 233–243.

Ginsberg, M.D., Feliciello, A., Jones, J.K., Avvedimento, E.V., and Gottesman, M.E. (2003). PKA-dependent binding of mRNA to the mitochondrial AKAP121 protein. J. Mol. Biol. *327*, 885–897.

Giorgio, V., Bisetto, E., Soriano, M.E., Dabbeni-Sala, F., Basso, E., Petronilli, V., Forte, M.A., Bernardi, P., and Lippe, G. (2009). Cyclophilin D modulates mitochondrial F0F1-ATP synthase by interacting with the lateral stalk of the complex. J. Biol. Chem. *284*, 33982–33988.

Giorgio, V., Soriano, M.E., Basso, E., Bisetto, E., Lippe, G., Forte, M.A., and Bernardi, P. (2010). Cyclophilin D in mitochondrial pathophysiology. Biochim. Biophys. Acta *1797*, 1113–1118.

Giorgio, V., Petronilli, V., Ghelli, A., Carelli, V., Rugolo, M., Lenaz, G., and Bernardi, P. (2012). The effects of idebenone on mitochondrial bioenergetics. Biochim. Biophys. Acta *1817*, 363–369.

Giorgio, V., von Stockum, S., Antoniel, M., Fabbro, A., Fogolari, F., Forte, M., Glick, G.D., Petronilli, V., Zoratti, M., Szabó, I., et al. (2013). Dimers of mitochondrial ATP synthase form the permeability transition pore. Proc. Natl. Acad. Sci. USA *110*, 5887–5892.

Giorgio, V., Burchell, V., Schiavone, M., Bassot, C., Minervini, G., Petronilli, V., Argenton, F., Forte, M., Tosatto, S., Lippe, G., and Bernardi, P. (2017). Ca^{2+} binding to F-ATP synthase β subunit triggers the mitochondrial permeability transition. EMBO Rep. *18*, 1065–1076.

Giorgio, V., Guo, L., Bassot, C., Petronilli, V., and Bernardi, P. (2018). Calcium and regulation of the mitochondrial permeability transition. Cell Calcium *70*, 56–63.

Giraud, M.F., Paumard, P., Soubannier, V., Vaillier, J., Arselin, G., Salin, B., Schaeffer, J., Brèthes, D., di Rago, J.P., and Velours, J. (2002). Is there a relationship between the supramolecular organization of the mitochondrial ATP synthase and the formation of cristae? Biochim. Biophys. Acta *1555*, 174–180.

Green, D.W., and Grover, G.J. (2000). The IF(1) inhibitor protein of the mitochondrial F(1)F(0)-ATPase. Biochim. Biophys. Acta *1458*, 343–355.

Gu, J., Zhang, L., Zong, S., Guo, R., Liu, T., Yi, J., Wang, P., Zhuo, W., and Yang, M. (2019). Cryo-EM structure of the mammalian ATP synthase tetramer bound with inhibitory protein IF1. Science *364*, 1068–1075.

Guo, H., Bueler, S.A., and Rubinstein, J.L. (2017). Atomic model for the dimeric F_O region of mitochondrial ATP synthase. Science *358*, 936–940.

Guo, L., Carraro, M., Sartori, G., Minervini, G., Eriksson, O., Petronilli, V., and Bernardi, P. (2018). Arginine 107 of yeast ATP synthase subunit g mediates sensitivity of the mitochondrial permeability transition to phenylglyoxal. J. Biol. Chem. *293*, 14632–14645.

Guo, L., Carraro, M., Carrer, A., Minervini, G., Urbani, A., Masgras, I., Tosatto, S.C.E., Szabò, I., Bernardi, P., and Lippe, G. (2019). Arg-8 of yeast subunit e contributes to the stability of F-ATP synthase dimers and to the generation of the full-conductance mitochondrial megachannel. J. Biol. Chem. *294*, 10987–10997.

Habersetzer, J., Larrieu, I., Priault, M., Salin, B., Rossignol, R., Brèthes, D., and Paumard, P. (2013). Human F1F0 ATP synthase, mitochondrial ultrastructure and OXPHOS impairment: a (super-)complex matter? PLoS ONE *8*, e75429.

Hahn, A., Parey, K., Bublitz, M., Mills, D.J., Zickermann, V., Vonck, J., Kühlbrandt, W., and Meier, T. (2016). Structure of a Complete ATP Synthase Dimer Reveals the Molecular Basis of Inner Mitochondrial Membrane Morphology. Mol. Cell *63*, 445–456.

Harris, D.A. (1993). The 'non-exchangeable' nucleotides of F1-F0ATP synthase. Cofactors in hydrolysis? FEBS Lett. *316*, 209–215.

He, J., Carroll, J., Ding, S., Fearnley, I.M., and Walker, J.E. (2017a). Permeability transition in human mitochondria persists in the absence of peripheral stalk subunits of ATP synthase. Proc. Natl. Acad. Sci. USA *114*, 9086–9091.

He, J., Ford, H.C., Carroll, J., Ding, S., Fearnley, I.M., and Walker, J.E. (2017b). Persistence of the mitochondrial permeability transition in the absence of subunit c of human ATP synthase. Proc. Natl. Acad. Sci. USA *114*, 3409–3414.

He, J., Ford, H.C., Carroll, J., Douglas, C., Gonzales, E., Ding, S., Fearnley, I.M., and Walker, J.E. (2018). Assembly of the membrane domain of ATP synthase in human mitochondria. Proc. Natl. Acad. Sci. USA *115*, 2988–2993.

Heyrovská, R. (1989). Effective radii of alkali halide ions in aqueous solutions, crystals and in the gas phase and the interpretation of stokes radii. Chem. Phys. Lett. *163*, 207–211.

Kühlbrandt, W., and Davies, K.M. (2016). Rotary ATPases: A New Twist to an Ancient Machine. Trends Biochem. Sci. *41*, 106–116.

Lapuente-Brun, E., Moreno-Loshuertos, R., Acín-Pérez, R., Latorre-Pellicer, A., Colás, C., Balsa, E., Perales-Clemente, E., Quirós, P.M., Calvo, E., Rodríguez-Hernández, M.A., et al. (2013). Supercomplex assembly determines electron flux in the mitochondrial electron transport chain. Science *340*, 1567–1570.

Lee, J., Ding, S., Walpole, T.B., Holding, A.N., Montgomery, M.G., Fearnley, I.M., and Walker, J.E. (2015). Organization of subunits in the membrane domain of the bovine F-ATPase revealed by covalent cross-linking. J. Biol. Chem. *290*, 13308–13320.

Lee, C.F., Chavez, J.D., Garcia-Menendez, L., Choi, Y., Roe, N.D., Chiao, Y.A., Edgar, J.S., Goo, Y.A., Goodlett, D.R., Bruce, J.E., and Tian, R. (2016). Normalization of NAD+ Redox Balance as a Therapy for Heart Failure. Circulation *134*, 883–894.

Lobo-Jarne, T., and Ugalde, C. (2018). Respiratory chain supercomplexes: Structures, function and biogenesis. Semin. Cell Dev. Biol. *76*, 179–190.

Massari, S., and Azzone, G.F. (1972). The equivalent pore radius of intact and damaged mitochondria and the mechanism of active shrinkage. Biochim. Biophys. Acta *283*, 23–29.

Mitchell, P. (1961). Coupling of phosphorylation to electron and hydrogen transfer by a chemi-osmotic type of mechanism. Nature *191*, 144–148.

Mnatsakanyan, N., Llaguno, M.C., Yang, Y., Yan, Y., Weber, J., Sigworth, F.J., and Jonas, E.A. (2019). A mitochondrial megachannel resides in monomeric F_1F_O ATP synthase. Nat. Commun. *10*, 5823–5834.

Myers, D.K., and Slater, E.C. (1957a). The enzymic hydrolysis of adenosine triphosphate by liver mitochondria. I. Activities at different pH values. Biochem. J. *67*, 558–572.

Myers, D.K., and Slater, E.C. (1957b). The enzymic hydrolysis of adenosine triphosphate by liver mitochondria. 2. Effect of inhibitors and added cofactors. Biochem. J. *67*, 572–578.

Neginskaya, M.A., Solesio, M.E., Berezhnaya, E.V., Amodeo, G.F., Mnatsakanyan, N., Jonas, E.A., and Pavlov, E.V. (2019). ATP Synthase C-Subunit-Deficient Mitochondria Have a Small Cyclosporine A-Sensitive Channel, but Lack the Permeability Transition Pore. Cell Rep. *26*, 11–17.e2.

Notredame, C., Higgins, D.G., and Heringa, J. (2000). T-Coffee: A novel method for fast and accurate multiple sequence alignment. J. Mol. Biol. *302*, 205–217.

Nuskova, H., Mikesova, J., Efimova, I., Pecinova, A., Pecina, P., Drahota, Z., Houstek, J., and Mracek, T. (2020). Biochemical thresholds for pathological presentation of ATP synthase deficiencies. Biochem. Biophys. Res. Commun. *521*, 1036–1041.

Petronilli, V., Szabò, I., and Zoratti, M. (1989). The inner mitochondrial membrane contains ion-conducting channels similar to those found in bacteria. FEBS Lett. *259*, 137–143.

Petronilli, V., Cola, C., Massari, S., Colonna, R., and Bernardi, P. (1993). Physiological effectors modify voltage sensing by the cyclosporin A-sensitive permeability transition pore of mitochondria. J. Biol. Chem. *268*, 21939–21945.

Pettersen, E.F., Goddard, T.D., Huang, C.C., Couch, G.S., Greenblatt, D.M., Meng, E.C., and Ferrin, T.E. (2004). UCSF Chimera–a visualization system for exploratory research and analysis. J. Comput. Chem. *25*, 1605–1612.

Pfeiffer, D.R., Gudz, T.I., Novgorodov, S.A., and Erdahl, W.L. (1995). The peptide mastoparan is a potent facilitator of the mitochondrial permeability transition. J. Biol. Chem. *270*, 4923–4932.

Pinke, G., Zhou, L., and Sazanov, L.A. (2020). Cryo-EM structure of the entire mammalian F-type ATP synthase. Nat. Struct. Mol. Biol. *27*, 1077–1085.

Piovesan, D., Minervini, G., and Tosatto, S.C. (2016). The RING 2.0 web server for high quality residue interaction networks. Nucleic Acids Res. *44* (*W1*), W367-74.

Rees, D.M., Leslie, A.G., and Walker, J.E. (2009). The structure of the membrane extrinsic region of bovine ATP synthase. Proc. Natl. Acad. Sci. USA *106*, 21597–21601.

Rizzuto, R., Simpson, A.W.M., Brini, M., and Pozzan, T. (1992). Rapid changes of mitochondrial Ca2+ revealed by specifically targeted recombinant aequorin. Nature *358*, 325–327.

Roy, S., Šileikytė, J., Schiavone, M., Neuenswander, B., Argenton, F., Aubé, J., Hedrick, M.P., Chung, T.D.Y., Forte, M.A., Bernardi, P., and Schoenen, F.J. (2015). Discovery, Synthesis, and Optimization of Diarylisoxazole-3-carboxamides as Potent Inhibitors of the Mitochondrial Permeability Transition Pore. ChemMedChem *10*, 1655–1671.

Salminen, T.S., Oliveira, M.T., Cannino, G., Lillsunde, P., Jacobs, H.T., and Kaguni, L.S. (2017). Mitochondrial genotype modulates mtDNA copy number and organismal phenotype in Drosophila. Mitochondrion *34*, 75–83.

Schägger, H., Cramer, W.A., and von Jagow, G. (1994). Analysis of molecular masses and oligomeric states of protein complexes by blue native electrophoresis and isolation of membrane protein complexes by two-dimensional native electrophoresis. Anal. Biochem. *217*, 220–230.

Scorrano, L., Penzo, D., Petronilli, V., Pagano, F., and Bernardi, P. (2001). Arachidonic acid causes cell death through the mitochondrial permeability transition. Implications for tumor necrosis factor-α aopototic signaling. J. Biol. Chem. *276*, 12035–12040.

Spannagel, C., Vaillier, J., Arselin, G., Graves, P.V., and Velours, J. (1997). The subunit f of mitochondrial yeast ATP synthase–characterization of the protein and disruption of the structural gene ATP17. Eur. J. Biochem. *247*, 1111–1117.

Spikes, T.E., Montgomery, M.G., and Walker, J.E. (2020). Structure of the dimeric ATP synthase from bovine mitochondria. Proc. Natl. Acad. Sci. USA *117*, 23519–23526.

Srivastava, A.P., Luo, M., Zhou, W., Symersky, J., Bai, D., Chambers, M.G., Faraldo-Gómez, J.D., Liao, M., and Mueller, D.M. (2018). High-resolution cryo-EM analysis of the yeast ATP synthase in a lipid membrane. Science *360*, eaas9699.

Stephan, T., Brüser, C., Deckers, M., Steyer, A.M., Balzarotti, F., Barbot, M., Behr, T.S., Heim, G., Hübner, W., Ilgen, P., et al. (2020). MICOS assembly controls mitochondrial inner membrane remodeling and crista junction redistribution to mediate cristae formation. EMBO J. *39*, e104105.

Stock, D., Leslie, A.G.W., and Walker, J.E. (1999). Molecular architecture of the rotary motor in ATP synthase. Science *286*, 1700–1705.

Strauss, M., Hofhaus, G., Schröder, R.R., and Kühlbrandt, W. (2008). Dimer ribbons of ATP synthase shape the inner mitochondrial membrane. EMBO J. *27*, 1154–1160.

Szabó, I., and Zoratti, M. (1991). The giant channel of the inner mitochondrial membrane is inhibited by cyclosporin A. J. Biol. Chem. *266*, 3376–3379.

Szabó, I., Bernardi, P., and Zoratti, M. (1992). Modulation of the mitochondrial megachannel by divalent cations and protons. J. Biol. Chem. *267*, 2940–2946.

Taylor, R.W., and Turnbull, D.M. (2005). Mitochondrial DNA mutations in human disease. Nat. Rev. Genet. *6*, 389–402.

Urbani, A., Giorgio, V., Carrer, A., Franchin, C., Arrigoni, G., Jiko, C., Abe, K., Maeda, S., Shinzawa-Itoh, K., Bogers, J.F.M., et al. (2019). Purified F-ATP synthase forms a Ca^{2+}-dependent high-conductance channel matching the mitochondrial permeability transition pore. Nat. Commun. *10*, 4341–4352.

Velours, J., Spannagel, C., Chaignepain, S., Vaillier, J., Arselin, G., Graves, P.V., Velours, G., and Camougrand, N. (1998). Topography of the yeast ATP synthase F0 sector. Biochimie *80*, 793–801.

Velours, J., Dautant, A., Salin, B., Sagot, I., and Brèthes, D. (2009). Mitochondrial F1F0-ATP synthase and organellar internal architecture. Int. J. Biochem. Cell Biol. *41*, 1783–1789.

von Stockum, S., Giorgio, V., Trevisan, E., Lippe, G., Glick, G.D., Forte, M.A., Da-Rè, C., Checchetto, V., Mazzotta, G., Costa, R., et al. (2015). F-ATPase of Drosophila melanogaster forms 53-picosiemen (53-pS) channels responsible for mitochondrial Ca2+-induced Ca2+ release. J. Biol. Chem. *290*, 4537–4544.

Waterhouse, A.M., Procter, J.B., Martin, D.M., Clamp, M., and Barton, G.J. (2009). Jalview Version 2–a multiple sequence alignment editor and analysis workbench. Bioinformatics *25*, 1189–1191.

Weimann, T., Vaillier, J., Salin, B., and Velours, J. (2008). The intermembrane space loop of subunit b (4) is a major determinant of the stability of yeast oligomeric ATP synthases. Biochemistry *47*, 3556–3563.

Wittig, I., Velours, J., Stuart, R., and Schägger, H. (2008). Characterization of domain interfaces in monomeric and dimeric ATP synthase. Mol. Cell. Proteomics *7*, 995–1004.

Wittig, I., Meyer, B., Heide, H., Steger, M., Bleier, L., Wumaier, Z., Karas, M., and Schägger, H. (2010). Assembly and oligomerization of human ATP synthase lacking mitochondrial subunits a and A6L. Biochim. Biophys. Acta *1797*, 1004–1011.

Zick, M., Rabl, R., and Reichert, A.S. (2009). Cristae formation-linking ultrastructure and function of mitochondria. Biochim. Biophys. Acta *1793*, 5–19.

STAR★METHODS

KEY RESOURCES TABLE

REAGENT or RESOURCE	SOURCE	IDENTIFIER
Antibodies		
Five mouse monoclonal anti-OXPHOS	Abcam	Cat# ab110411; RRID:AB_2756818
Rabbit polyclonal anti-citrate synthetase	Abcam	Cat# ab96600; RRID:AB_10678258
Mouse monoclonal anti-α subunit	Abcam	Cat# ab110273; RRID:AB_10858175
Mouse monoclonal anti-β subunit	Abcam	Cat# ab14730; RRID:AB_301438
Mouse monoclonal anti-b subunit	Abcam	Cat# ab117991; RRID:AB_10901555
Mouse monoclonal anti-OSCP subunit	Abcam	Cat# ab110276; RRID:AB_10887942
Rabbit polyclonal anti-g subunit	Abcam	Cat# ab126181; RRID:AB_11129974
Rabbit polyclonal anti-f subunit	Abcam	Cat# ab103951; RRID:AB_10711131
Mouse monoclonal anti-e subunit	Abcam	Cat# ab54879; RRID:AB_940392
Mouse monoclonal anti-IF1	Abcam	Cat# ab110277; RRID:AB_10861497
Mouse monoclonal anti-CyPD	Abcam	Cat# ab110324; RRID:AB_10864110
Rabbit recombinant anti-NDUFs1	Abcam	Cat#ab157221; RRID:AB_2857900
Rabbit polyclonal anti-GLS1	Abcam	Cat#ab93434; RRID:AB_10561964
Rabbit polyclonal anti-ANT3 (SLC25A6)	Abcam	Cat#ab154007; RRID:AB_2619664
Mouse monoclonal anti-Mic60 (mitofilin)	Abcam	Cat#ab110329; RRID:AB_10859613
Rabbit polyclonal anti-mic19	Abcam	Cat#ab224565; Immunogen: Q9NX63
Mouse monoclonal anti-SDHA	Santa Cruz	Cat#sc-166947; RRID:AB_10610526
Rabbit polyclonal anti-mic27 (apolipoprotein O like)	Genetex	Cat#GTX87433; RRID:AB_10725525
Rabbit polyclonal anti-γ subunit	Genetex	Cat# GTX114275; RRID:AB_10619344
Rabbit monoclonal anti-MPC1	Cell Signaling	Cat#D2L9I-14462; RRID:AB_2773729
Rabbit monoclonal anti-GAPDH	Cell Signaling	Cat#2118; RRID:AB_561053
Mouse monoclonal anti-mic10 (C1orf151)	ThermoFisher Scientific	Cat#MA5-26031; RRID:AB_2724017
Mouse monoclonal anti-prohibitin	ThermoFisher Scientific	Cat# MS-261-P1; RRID:AB_61896
Chemicals, peptides, and recombinant proteins		
Digitonin	Calbiochem	300410
Digitonin	Sigma-Aldrich	D141
Oligomycin-A	Merck	495455
Rotenone	Sigma-Aldrich	R8875
Antimycin A	Sigma-Aldrich	A8674
carbonylcyanide-p-trifluoromethoxyphenyl hydrazine (FCCP)	Sigma-Aldrich	C2920
Puromycin	Sigma Aldrich	P7255
Alamethicin	Sigma-Aldrich	A4665
Arachidonic Acid Sodium Salt	Sigma-Aldrich	A8798
Protease inhibitor	Sigma-Aldrich	P8340
Tetramethylrhodamine, Methyl Ester, Perchlorate (TMRM)	Invitrogen	T668
Nonyl Acridine Orange (NAO)	Sigma-Aldrich	A7847
Cyclosporin H	AdipoGen life Sciences	AG-CN2-0447-M005
Cyclosporin A	Sigma-Aldrich	C3662
Ca^{2+} green	Invitrogen	C3737
Pyruvate Kinase	Sigma-Aldrich	P1506

(*Continued on next page*)

Continued

REAGENT or RESOURCE	SOURCE	IDENTIFIER
Lactate dehydrogenase	Sigma-Aldrich	L2625
Phosphoenolpyruvic acid	Sigma-Aldrich	P7127
Critical commercial assays		
Pierce BCA Protein Assay Kit	Thermo Fisher Scientific	23225
Experimental models: Cell lines		
HEK293T	ATCC	N/A
HeLa	ATCC	N/A
Oligonucleotides		
shRNA sequence: ATP5J2 #sh1: CCGGGTACCAGTGAAGGACAAGAAA CTCGAGTTTCTTGTCCTTCACTGGTACTTTTTG	Sigma-Aldrich	TRCN0000038261
shRNA sequence: ATP5J2 #sh2: CCGGCCGGTACTACAACAAGTAC ATCTCGAGATGTACTTGTTGTAGTA CCGGTTTTTG	Sigma-Aldrich	TRCN0000038259
shRNA sequence: ATP5J2 #sh3: CCGGCTGGATCTTGATGCGGGA CTTCTCGAGAAGTCCCGCATCAA GATCCAGTTTTTG	Sigma-Aldrich	TRCN0000038263
shRNA sequence: ATP5J2 #sh4: CCGGCGGAGCGTTTCAAAGAG GTTACTCGAGTAACCTCTTTGA AACGCTCCGTTTTTG	Sigma-Aldrich	TRCN0000038262
shRNA sequence: ATP5J2 #sh5: CCGGCGGAGCGTTTCAAAGAGG TTACTCGAGTAACCTCTTTGAA ACGCTCCGTTTTTG	Sigma-Aldrich	TRCN0000038260
shRNA-resistant *ATP5J2* pcDNA: atgtccgtcctgacgccgctgctgctgcg gggcttgacaggctcggcccggcggctcc cagtgccgcgcgccaaggcgtcagttggtga gtgtccggccccagtaccagtgaaggacaa gaaacttctggaggtcaaactgggggagct gccaagctggatcttgatgcgggacttcagt cctagtggcatttttggggctttccagcgcgg ctattaccggtactacaacaagtacatcaatg tgaagaaggggagcatctcggggattac catggtgctggcatgctacgtgctctttagc tactccttttcctacaagcatctcaagcac gagcggctccgcaaataccactga	Sigma-Aldrich	GeneArt Gene Synthesis service
Recombinant DNA		
pLKO.1 lentiviral vector	Sigma-Aldrich	SHC001
pLKO.1 + shRNA (1-5)	Sigma-Aldrich	SHCLNG-NM_004889 (bacterial stock)
pcDNA3.1 vector	Invitrogen	V79020
Software and algorithms		
UCSF Chimera	Pettersen et al., 2004	https://www.cgl.ucsf.edu/chimera/
SWISS-MODEL	Bienert et al., 2017	https://swissmodel.expasy.org/
RING 2.0	Piovesan et al., 2016	http://old.protein.bio.unipd.it/ring/
Uniprot	Bateman et al., 2017	https://www.uniprot.org/
T-coffee	Notredame et al., 2000	https://www.ebi.ac.uk/Tools/msa/tcoffee/
Jalview	Waterhouse et al., 2009	https://www.jalview.org/

(*Continued on next page*)

Continued

REAGENT or RESOURCE	SOURCE	IDENTIFIER
ImageJ	National Institutes of Health (NIH)	https://imagej.nih.gov/ij/download.html
Origin8	Origin Lab	https://www.originlab.com/
Prism8	GraphPad	https://www.graphpad.com/

RESOURCE AVAILABILITY

Lead contact

Further information and requests for resources and reagents should be directed to and will be fulfilled by the Lead Contact, Valentina Giorgio (valentina.giorgio4@unibo.it).

Materials availability

This study did not generate new unique reagents.

Data and code availability

This study did not generate new unique datasets/code.

EXPERIMENTAL MODEL AND SUBJECT DETAILS

HeLa cells were obtained from the American Tissue Culture Collection (ATCC); CTR, sh2 and sh5 f KD HeLa cells were cultured in Dulbecco's modified Eagle's medium (DMEM; Lonza, Basel, Switzerland), and supplemented with fetal bovine serum (10% v/v), glutamine (4 mM), penicillin and streptomycin (ThermoFisher Scientific, Massachusetts, USA). Glucose deprivation was obtained by culturing CTR, sh2 and sh5 f KD in a low glucose-containing DMEM medium (LG). LG medium was prepared with a DMEM glucose free (Thermo Fisher Scientific, Massachusetts, USA) supplemented with fetal bovine serum (10% v/v), glutamine (4 mM), penicillin, streptomycin (Thermo Fisher Scientific, Massachusetts, USA), 2.5 mM glucose, 5 mM and pyruvate. High glucose-containing (HG) medium was obtained as above, with the addition of 25 mM glucose. Cells were free of contamination with mycoplasma, as routinely tested. Cells were grown at 37°C in a 5% CO_2 humidified incubator.

METHODS DETAILS

Stable knocking down of the f subunit

Stable interference of the f subunit was obtained by HeLa transfection with a panel of shRNAs (sh1-sh5, Sigma) cloned into the pLKO.1 lentiviral vector and targeting the human f subunit mRNA:

sh1)CGGGTACCAGTGAAGGACAAGAAACTCGAGTTTCTTGTCCTTCACTGGTACTTTTTG;sh2)CGGCCGGTACTACAACAAG-TACATCTCGAGATGTACTTGTTGTAGTACCGGTTTTTG;sh3)CGGCTGGATCTTGATGCGGGACTTCTCGAGAAGTCCCGCAT-CAAGATCCAGTTTTTG;sh4)CGGCGTGCTCTTTAGCTACTCCTTCTCGAGAAGGAGTAGCTAAAGAGCACGTTTTTG;sh5) CGGCGGAGCGTTTCAAAGAGGTTACTCGAGTAACCTCTTTGAAACGCTCCGTTTTTG. This panel of shRNA plasmids were co-transfected with the three packaging plasmids pMDLg/pRRE, pRSV-Rev and pMD2.G into HEK293T cells for viral production. Recombinant virus was collected and used to infect HeLa cells. Empty vector pLKO.1 (SHC001 Sigma) was used as control. Cells were selected in 0.8 μg/ml puromycin for a stable knocking down and analyzed by Western Blotting. The selected mixed cell populations did not follow single-cell cloning procedure.

Transient f subunit re-expression

Transient re-expression of the f subunit was achieved by transfection of sh5 f KD HeLa cells with a pcDNA3.1 containing shRNA5-resistant *ATP5J2* pcDNA. The pcDNA3.1 containing shRNA-resistant *ATP5J2* pcDNA was purchased from Sigma (GeneArt Gene Synthesis service) and the full cDNA sequence inserted in the vector is:

atg*tccgtcctgacgccgctgctgctgcggggcttgacaggctcggcccggcggctcccagtgccgcgcgccaag*gcgtcagttggt-gagtgtccggccccagtaccagtgaaggacaagaaacttctggaggtcaaactgggggagctgccaagctggatcttgatgcgggactt-cagtcctagtggcatttt**tggggctttccagcgcggctatt**accggtactacaacaagtacatcaatgtgaagaaggggagcatctcggggat-taccatggtgctggcatgctacgtgctctttagctactccttttcctacaagcatctcaagcacgagcggctccgcaaataccactga.

This shRNA-resistant *ATP5J2* cDNA sequence was modified to introduce (i) the mitochondrial targeting sequence of *COX VIII* gene (shown in italics); (ii) silent mutations (shown as underlined characters) into the shRNA5 recognition sequence (shown in bold). CTR

and sh5 f KD HeLa cells, were transfected with the corresponding empty vector (EV), pcDNA3.1, purchased from Invitrogen, in order to generate proper experimental controls. HeLa cells transfection was achieved with the Ca^{2+} phosphate transfection protocol. Briefly, 4 μg (for the electron microscopy analysis) or 40 μg DNA (for the mitochondrial swelling experiment), were diluted in sterile H_2O to which 5 μL or 100 μL ice-cold 2.5 M $CaCl_2$ had been added. The DNA/Ca^{2+} mixture, final volume 50 μL or 1000 μl, was then added dropwise to 2 × HEPES-buffered saline (HBS) composed of 40 mM HEPES, 280 mM NaCl, and 1.5 mM Na_2HPO_4 (pH 7.18) while vortexing. The final mixture, was added dropwise to the cells and incubated at 37°C for 6 h. The medium was then removed, cells were washed repeatedly with phosphate-buffered saline (PBS) until no $Ca_3(PO_4)_2$ crystals remained, and fresh growth medium was added to the cells. After 48 hours post-transfection cells were either used for electron microscopy analysis or for mitochondrial swelling assay.

Growth curve

HeLa cells were seeded at 10000 (CTR, sh2 and sh5 f KD) cells/well in a 12 wells tissue culture plate in DMEM containing 25 mM glucose. Cells were incubated at 37°C in a 5% CO_2 humidified incubator and cultured for 96 hours. After 24, 48, 72 or 96 hours cells were harvested with trypsin and counted.

Lysates, gel electrophoresis, western blotting

Cells (10×10^6) were kept on ice for 20 min in a 0.15 mL of buffer containing 150 mM NaCl, 20 mM Tris, 5 mM EDTA-Tris, pH 7.4 with the addition of 1% (v/v) Triton X-100, 10% (v/v) glycerol and protease inhibitor cocktail (Merck, Darmstadt, Germany). Cell extracts were then cleared by centrifugation at 18,000 × g for 20 min, 4°C. Laemmli buffer (500 mM Tris-HCl, 50% v/v glycerol, 10% w/v SDS, 25% v/v β-mercaptoethanol and 0.2% w/v bromophenol blue, pH 6.8) was added to supernatants and samples were separated by a polyacrylamide gradient gel (NuPAGE, 12% Bis-Tris, Invitrogen) and transferred electrophoretically to nitrocellulose membranes. Blocking was performed in a PBS solution containing 5% (w/v) non-fat dry milk (PanReac Applichem). Antibodies for OXPHOS (OXPHOS Human WB Antibody Cocktail), Citrate Synthase, CyPD, IF1, Ndufs1, GLS1, ANT3, mic60, mic19 and for β, α, OSCP, b, f, e, g subunits were from Abcam (Cambridge, UK), for γ subunit or mic27 were from Genetex (California, USA), for SDHA was from Santa Cruz Biotechnology (Dallas, USA), for prohibitin and mic10 were from ThermoFischer Scientific (Massachusetts, USA) and the ones against MPC1 and GAPDH were from Cell Signaling (Massachusetts, USA). Detailed information on the specific antibodies used can be found on the key resource table. Band pixels of each replicate are normalized on band pixels of their proper loading control (citrate synthase or prohibitin). Mean pixel ratios ± SEM are then shown proportionally to the mean of CTR samples, expressed as 1.

Cell permeabilization, mitochondria preparation

HeLa cells were detached with trypsin, centrifuged at 1,000 × g for 5 min, and washed twice with PBS. The resulting pellet was re-suspended in KCl-based medium (130 mM KCl, 10 mM Mops-Tris, pH 7.4, containing 1 mM EGTA-Tris and 150 μM digitonin (D141) and was incubated for 20 min on ice. Cells were then diluted 1:10 in KCl medium containing 10 μM EGTA-Tris and centrifuged at 1,000 × g in a refrigerated centrifuge (4°C) for 5 min. The final pellet, containing permeabilized cells, was suspended and used for Mg^{2+}-ATP hydrolysis or CRC measurements.

Mitochondria from HeLa cells were obtained either after cell homogenization with a glass-Teflon potter as previously described (Frezza et al., 2007), or in the presence of digitonin (4mg/ml). In the first case mitochondria were used for swelling assay or for ATP synthase oligomerization analysis with BN-PAGE, while mitochondria prepared with digitonin were used for respiratory chain supercomplex analysis with BN-PAGE.

ATP hydrolysis

ATPase activity was measured monitoring the rate of oxidation of NADH of permeabilized HeLa cells at the concentration of 0.4×10^6 cells/well in a final volume of 0.2 ml. ATP- regenerating system contained 50 mM KCl, 50 mM Tris-HCl, 30 mM sucrose, 4 mM $MgCl_2$, 2 mM EGTA adjusted to pH 7.4 and was supplemented with 4 units/ml pyruvate kinase, 3 units/ml lactate dehydrogenase, 4 mM phosphoenolpyruvate, 2 mM ATP, 0.2 mM NADH, 10 μM alamethicin, and 10 μM sodium decavanadate. CTR, sh2 or sh5 f KD HeLa cells were permeabilized as described above and suspended in the ATP-regenerating system. NADH absorbance was measured spectrophotometrically at 340 nm, 37°C using a Fluoroskan Ascent FL (Thermo Electron, Waltham, MA, USA) plate reader. Inhibition of Mg^{2+}-ATPase activity was obtained by adding 2 μM oligomycin to wells.

Oxygen consumption

Oxygen consumption rate (OCR) in adherent cells were measured using the XF24 Extracellular Flux Analyzer (Agilent technologies) as in (Giorgio et al., 2012). HeLa cells were seeded in XF24 cell culture microplates at 50000 (CTR, sh2 or sh5 f KD) cells/well. Cells were incubated at 37°C in a 5% CO_2 humidified incubator for 24 h. Assay was initiated by replacing the growth medium with Seahorse medium (DMEM, Sigma D5030, supplemented with NaCl, glutamine and phenol red according to the manufacturer protocol and 25 mM (HG) or 2.5 mM (LG) glucose, 10 mM sodium pyruvate) prewarmed at 37°C. Cells were incubated at 37°C for 30 min to allow temperature and pH equilibration. A titration with FCCP was performed for each experiment to determine the optimal FCCP concentration that stimulates respiration maximally, which was found to be 0.1 μM for all cell types. After an OCR baseline was established, 1 μg/ml oligomycin, 0.1 μM FCCP, 1 μM rotenone, and 1 μM antimycin A were sequentially added to each well.

Nonyl Acridine Orange staining

Nonlyl Acridine Orange (NAO) staining has been used to measure the mitochondrial content in cells. The dye binds specifically cardiolipin in mitochondria. Cells, were seeded at 50000 cells/well in a 24-wells tissue culture plate. NAO dye (200 nM, Merck) was added to cells 24 h after seeding. Cells were stained for 30 min at 37°C, washed, detached with trypsin, centrifuged at 1,000 x g for 5 min, and suspended in the saline buffer. Mitochondrial mass was assessed by flow cytometry using the FACS Canto II flow cytometer (Becton Dickingson).

Blue native gel electrophoresis

For the respiratory chain supercomplex analysis, mitochondria from CTR, sh2, or sh5 f KD HeLa cells were resuspended in 100 μl of a buffer composed of 1.5 M aminocaproic acid, 50 mM Bis-Tris, pH 7.0, solubilized with 1% (w/v) digitonin, incubated on ice for 5 min and solubilized protein complexes were separated through centrifugation at 18,000 x g for 30 min at 4°C.

Supernatants were collected, supplemented with a sample buffer prepared with 5% (w/v) Serva Blue G, 1.0 M aminocaproic acid and quickly loaded onto a 3%–12% blue native polyacrylamide gradient gel (BN-PAGE, Invitrogen). After electrophoresis, gels were used for Complex I in gel-activity staining (Salminen et al., 2017) or Western Blotting against Ndufs1 (Complex I) or SDHA (Complex II) subunits.

For ATP synthase studies, freshly prepared mitochondria from CTR, or sh5 f KD HeLa cells were resuspended at the concentration of 10 mg/ml, in a buffer composed of 0.75 M aminocaproic acid, 50 mM Bis-Tris, pH 7.0 (Galber et al., 2019; Schägger et al., 1994). They were solubilized with different concentration of digitonin (1-2,5% (w/v)), and immediately centrifuged at 100,000 x g for 25 min at 4°C. Supernatants were collected, supplemented with a sample buffer prepared with 5% (w/v) Coomassie G, 0.5 M aminocaproic acid and quickly loaded onto a 3%–12% blue native polyacrylamide gradient gel (BN-PAGE, Invitrogen). After electrophoresis, gels were stained with colloidal Coomassie or used for ATP synthase in gel-activity staining (Bisetto et al., 2007) or Western Blotting against β subunit.

Electron Microscopy

HeLa cells were seeded at 30000 (CTR, sh2 and sh5 f KD, or CTR+EV, sh5 f KD+EV and sh5 f KD+f subunit) cells/well in a 24 well plate. Cells were incubated at 37°C in a 5% CO_2 humidified incubator and cultured for 24 h in order to reach 70%–80% of confluence. The day after, or 48 hours after Ca^{2+} phosphate transfection for f subunit re-expression, the growth medium was discarded; cells were washed with phosphate-buffered saline (PBS), fixed with 2.5% (v/v) glutaraldehyde in 0.1 M sodium cacodylate buffer, pH 7.4 for 1 hour at 4°C, and then incubated with a solution of 1% (v/v) of tannic acid for 1h. The samples were post-fixed with 1% (v/v) osmium tetroxide in 0.1 M sodium cacodylate buffer for 1 hour, 4°C. After three water washes, samples were dehydrated in a graded ethanol series and embedded in an epoxy resin (Sigma-Aldrich). Ultrathin sections (60-70 nm) were obtained with an Ultrotome V (LKB) ultramicrotome, counterstained with uranyl acetate and lead citrate and viewed with a Tecnai G2 (FEI) transmission electron microscope operating at 100 kV. Images were captured with a Veleta (Olympus Soft Imaging System) digital camera. Mitochondria were analyzed by counting the number of them containing at least one ''arch-like'' or ''longitudinal'' cristae structure. Mitochondria not displaying the described structures were considered ''normal.'' Cristae junctions per mitochondrion were quantified by monitoring the points of contact between the inner and the outer membrane in each mitochondrion.

Mitochondrial swelling

Changes of HeLa mitochondrial volume were followed in a 96-well clear assay plate (Falcon), final volume of 0.2 ml. Freshly prepared mitochondria from CTR, sh2 and sh5 f KD HeLa cells, or from CTR+EV, sh5 f KD+EV and sh5 f KD+f subunit HeLa cells, were suspended at the concentration of 0.5 mg/ml in a KCl-based medium (130 mM KCl, 10 mM MOPS-Tris, 10 μM EGTA), sucrose-based medium (0.2 M sucrose, 10 mM MOPS-Tris, 10 μM EGTA) or arabinose-based medium (0.2 M arabinose, 10 mM MOPS-Tris, 10 μM EGTA). For the size exclusion limit of the PTP, mitochondria were suspended in a polyethylene glycol (PEG) solution of equivalent osmatic pressure (supplemented with 10 mM MOPS-Tris, 10 μM EGTA). PEG molecules of increasing molecular weight (200, 400, 600, 1500) were added to 30% by volume to the sucrose-based medium as in (Carroll et al., 2019; Pfeiffer et al., 1995). Each of the aforementioned media, was supplemented with 5 mM succinate-Tris and 1 mM Pi-Tris. Absorbance was measured at 540 nm for 5 min in order to reach stable values, using a Multiskan EX (Thermo Scientific) plate reader. Then, different concentration of Ca^{2+} (25-50-100 μM for the KCl- and sucrose-based media and 50 μM for the arabinose- and PEG-based media or for the sucrose-based medium in the f subunit re-expression experiment) were added to induce mitochondrial swelling and the absorbance changes were followed for 30 min. At the end of each experiment alamethicin (10 μM, or 30 μM in PEG solutions) was added to get the maximal mitochondrial swelling. Fraction of swollen mitochondria is calculated as in Petronilli et al. (1993).

Specific time points to quantify the fraction of swollen mitochondria of different traces are chosen based on the time at which the fraction of CTR swollen mitochondria is equivalent to 50%, after 50 μM Ca^{2+}addition in each experiment, in sucrose- (Figures 4C and 4E) or in PEG 200-based media (Figure S1D). Data are presented as mean ± SEM.

Ca^{2+} retention capacity

For the Calcium Retention Capacity (CRC) assay, external mitochondrial Ca^{2+} was measured by Ca^{2+} Green-5N fluorescence using a Fluoroskan Ascent FL (Thermo Electron, Waltham, MA, USA) plate reader. CTR, sh2 or sh5 cells were permeabilized and were

resuspended at the concentration of $10^6 \times ml^{-1}$ in a KCl- based medium (130 mM KCl, 10 mM MOPS-Tris, 10 μM EGTA) or sucrose-based medium (0.2 M sucrose, 10 mM MOPS-Tris, 10 μM EGTA) supplemented with 5 mM succinate-Tris, 1 mM Pi-Tris and 0.5 μM Ca^{2+} Green-5N, pH 7.4 to a final volume of 0.2 ml. For all CRC measurements, sequential 2.5 μM $CaCl_2$ pulses were added to cells.

Mitochondrial membrane potential

To measure the mitochondrial membrane potential, 30000 cells (CTR, sh5 f KD) were seeded onto 24 mm-diameter round glass coverslips and grown for 2 days in DMEM. For the analysis, cells were incubated in bicarbonate- and phenol red-free Hanks' Balanced Salt solution (HBSS, Merck) containing 10 mM HEPES, 1.6 μM cyclosporin H to inhibit the multidrug resistance pump (Bernardi et al., 1999), 20 nM TMRM, pH 7.4. When required, CTR, sh5 f KD cells were incubated with compound 63 (1 μM) or CsA (3.2 μM) to inhibit permeability transition (Broekemeier et al., 1989; Roy et al., 2015). Mitochondrial membrane potential was measured based on the accumulation of TMRM and was read for about 10 min to get stable values. Then, arachidonic acid (5, 8, 10 μM) was added to induce mitochondrial depolarization. At the end of each experiment, mitochondria were fully depolarized by the addition of FCCP (5 μM). Recordings were performed every 2 minutes using an Olympus IX71/IX51 inverted microscope equipped with a xenon light source (150W) for epifluorescence illumination and with a digital camera. For detection of fluorescence 545 nm bandpass excitation and 573 nm longpass emission filter settings were used for TMRM. Images were collected with an exposure time of 120 ms (33% illumination intensity) using a 40 ×, 1.3 NA oil immersion objective (Olympus). Data were acquired and analyzed using ImageJ and GraphPad software. Fields not containing cells were taken as the background.

Structure analysis of the human f subunit

The 3D structure of dimeric Fo from *S.* (PDBid: 6B2Z) and the bovine counterpart (PDBid: 6ZBB) were inspected with Chimera (Pettersen et al., 2004). The 3D structure of the human f subunit was predicted with SWISS-MODEL (Bienert et al., 2017), selecting 6ZBB:chain f as template. Networks of interacting residues were calculated with RING 2.0 (Piovesan et al., 2016). The sequences of the f subunit from *S. cerevisiae*, *Y. lipolytica*, *B. taurus, S. scrofa* and *Homo sapiens* were retrieved from Uniprot (Bateman et al., 2017), aligned with T-coffee (Notredame et al., 2000) and visualized with Jalview (Waterhouse et al., 2009).

QUANTIFICATION AND STATISTICAL ANALYSIS

Unless otherwise stated in the figure legends, each experiment was repeated at least three times. Data are presented as mean ± SEM, or, for clarity, as representative experiments (see figure legends for details). *P value*s indicated in the figures are calculated with GraphPad, *Student's t-test* is applied (* represents $p \leq 0.05$, ** $p \leq 0.01$, *** $p \leq 0.001$). Western blot band intensities and mitochondrial membrane potential measurements were analyzed using ImageJ and GraphPad software.